Inorganica Chimica Acta 478 (2018) 59–70

Contents lists available at ScienceDirect

Inorganica Chimica Acta

journal homepage: www.elsevier.com/locate/ica

Research paper

Sev and pcu topological nets in one-pot newly synthesized mixed-ligand imidazole-containing Cu(II) coordination frameworks: Crystal structure, intermolecular interactions, theoretical calculations, magnetic behavior and biological activity

Amani Direm [a,*], Mohammed S.M. Abdelbaky [b], Koray Sayın [c], Andrea Cornia [d], Olufunso Abosede [e], Santiago García-Granda [b]

[a] Laboratoire des Structures, Propriétés et Interactions Interatomiques LASPI²A, Département des Sciences de la Matière, Faculté des Sciences et de la Technologie, Université "Abbes Laghrour", Khenchela 40.000, Algeria
[b] Departamento de Química Física y Analítica, Universidad de Oviedo CINN, 33006 Oviedo, Spain
[c] Department of Chemistry, Faculty of Science, Cumhuriyet University 58140 Sivas, Turkey
[d] Dipartimento di Scienze Chimiche e Geologiche, Università di Modena e Reggio Emilia & INSTM, via G. Campi 103, 41125 Modena, Italy
[e] Department of Chemistry, Federal University Otuoke, P.M.B 126, Yenagoa, Bayelsa State, Nigeria

ARTICLE INFO

Article history:
Received 30 November 2017
Received in revised form 3 February 2018
Accepted 9 March 2018
Available online 30 March 2018

Keywords:
Coordination networks
Imidazole-based copper complexes
One-pot synthesis
Crystal structure
*Hirshfeld*surface analysis
Topological analysis
Ab-initio calculations
Magnetic properties
Biological properties

ABSTRACT

Novel mixed-ligand coordination frameworks, occurring concomitantly namely $[Cu(Im)_3(H_2Cit)]$ (**1**) and $[Cu(Im)_2(HCit)]\cdot HIm$ (**2**) (with Im = imidazole and H_4Cit = citric acid) were obtained as a result of the one-pot reaction between imidazole, citric acid and copper chloride. The complexes were structurally characterized by elemental analysis, FTIR spectroscopy and X-ray diffraction. The two structures were found to be connected through 3D hydrogen-bonding networks examined by means of the *Hirshfeld* surface analysis which highlighted the presence of O–H···O, N–H···O and C–H···O H-bonds together with the $\pi\cdots lp$ interactions. A topological analysis of the underlying nets corresponding to the two hydrogen-bonded frameworks was carried out. Moreover, quantum chemical calculations were performed using the HF method with 6-31G(d) and LANL2DZ levels in the gas phase, and therefore the optimized structures, the IR, ^1H NMR, ^{13}C NMR spectra and the electronic structure descriptors were examined in detail. Furthermore, the magnetic properties of (**1**) and (**2**) were also investigated. The complexes showed remarkable antimicrobial and antifungal inhibition activities.

1. Introduction

The nitrogen atoms of the imidazole ring bear interesting physical and chemical properties that result in different pharmacological activities of the molecule and its derivatives [1]. Imidazole and its derivatives have been reported to have analgesic, anti-inflammatory, cardiovascular, anti-neoplastic, antifungal, enzyme inhibition, antiviral and antiulcer activities [2]. Moreover, the anti-parasitic and antiviral activities of aniline derivatives of imidazole have been described in the literature [3].

Imidazole occurs in most proteins as part of the side chain of histidine and constitutes a binding site for various transition metal ions in a large number of metalloproteins [4]. Consequently, the bonding between imidazole and transition metal ions is widely known [5] and of considerable interest especially in biological systems [6,7]. In order to understand the special magnetic and spectroscopic properties and the catalytic mechanisms of copper proteins, the study and modeling of the active site of copper-containing proteins has been a field of great interest within the scientific community [8]. Therefore, copper(II)–imidazole systems with different ratios of imidazole to copper have been prepared and investigated by several researchers [9]. Furthermore, being studied as models for copper proteins that contain both functionalities in the side chain [10], some mononuclear copper(II)–imidazole complexes with carboxylate ligands have been found to display a variety of pharmacological effects, including antitumor [11], superoxide dismutase and catecholase activities [12]. In particular, the recognition of the strong antitumor activity of the trans bis

* Corresponding author.
E-mail address: amani_direm@yahoo.fr (A. Direm).

https://doi.org/10.1016/j.ica.2018.03.011
0020-1693/

(acetato) bis(imidazole) copper(II) complex [13] caused a growing interest in the synthesis and characterization of these systems [14].

Despite the huge number of papers on imidazole complexes involving different carboxylates and different metallic centers (copper [15], cobalt [16], nickel [16d,17], manganese [17d,18], cadmium [19] and ruthenium [20]), the crystallographic information about imidazole-based complexes containing citrate ligands is rather scarce; only two hexacoordinated complexes have been reported until now, namely $[M(Im)_6][M_\Delta(Im)_3(Hcit)][M_\Lambda(Im)_3(Hcit)]\cdot 4H_2O$ with (M = Co/Ni, Im = imidazole, H_4cit = citric acid) [21]). As a contribution to this study, we present herein an investigation of two new penta-coordinated copper(II) complexes with mixed-ligands: imidazole and citric acid.

2. Experimental

2.1. Synthesis

Equimolar quantities of imidazole (0.136 g, 2 mmol), citric acid (0.384 g, 2 mmol) and $CuCl_2$ (0.268 g, 2 mmol) were mixed together with 20 mL of ethanol in a one-pot reaction. The mixture was stirred at 60 °C for one hour and the resulting blue-colored solution was filtered and left at room temperature for several days, leading to two concomitant complexes: light blue-green prisms of $[Cu(Im)_3(H_2Cit)]$ (**1**) and blue prismatic crystals of $[Cu(Im)_2(HCit)]\cdot HIm$ (**2**). Elemental analysis (C, H and N) for (**1**) calc. (exp.): Cu 13.85, O 24.41, N 18.31 (18.48), C 39.26 (39.31), H 4.17 (4.32) %. Elemental analysis (C, H and N) for (**2**) calc. (exp.): Cu 13.85, O 24.41, N 18.31 (18.57), C 39.26 (39.35), H 4.17 (4.48)%.

2.2. Physical measurements

2.2.1. FTIR spectroscopy

The Fourier transform infrared spectra were recorded on a Perkin-Elmer FTIR spectrophotometer in the range of 4000–400 cm^{-1} by using KBr pellets at room temperature.

2.2.2. Elemental analyses

Elemental analyses (C, H and N) were performed using a Carlo Erba EA1110 CHNS-O automatic analyzer

2.2.3. Magnetic measurements

Magnetic measurements were performed using a Quantum Design PPMS magnetometer on 23.11- and 21.09-mg polycrystalline samples of (**1**) and (**2**), respectively, compacted and enclosed in a polypropylene holder. After zero-field cooling, temperature was scanned from 2 to 300 K and backward with an applied field of 1 kOe. Molar magnetic susceptibility (χ_M) data were calculated using a molar mass of 457.89 g mol^{-1} and a diamagnetic correction (evaluated from Pascal's constants [22]) of $-196.76\cdot10^{-6}$ emu mol^{-1} for both compounds. Measurements in heating and cooling mode showed no significant differences. No changes have been observed in the samples after performing the magnetic measurements. $\chi_M T$ values for (**1**) displayed only a slight increase with increasing temperature, presumably due to temperature independent paramagnetism or inaccuracy of diamagnetic correction (Fig. S1). A more distinct positive slope was instead observed for (**2**), a behavior that we attribute to an unidentified ferromagnetic impurity in the sample (Fig. S2).

2.3. X-ray single-crystal structure analysis

Single-crystal diffraction data were collected at room temperature on a Bruker-Nonius X8 APEX diffractometer with graphite-monochromated Mo Kα radiation (λ = 0.71073 Å). The data collection was performed with the software APEX2 [23]. Data integration and reduction were carried out with SAINT software [23], while absorption correction was applied with SADABS [23]. Calculations were carried out using the *WinGX* software package [24]. Structures were solved by direct methods using *SIR2014* [25] and refined by full-matrix least-squares methods against F^2 using *SHELXL2014* [26]. All non-hydrogen atoms were refined anisotropically. Hydrogen atoms were located on difference Fourier maps, placed in calculated positions and refined using a riding model, with distances constraints of N—H = 0.86 Å and C—H = 0.93 (aromatic-CH), 0.97 Å (citrate-CH_2) [U_{iso}(H) = 1.2 U_{eq}(N,C)]. Experimental conditions and X-ray structure information for both synthesized compounds are listed in Table S1. Crystal structures were visualized using *ORTEP-3* [24] and *MERCURY* [27]. Material for publication was prepared with *WinGX* [24] and *publCIF* [28].

2.4. Theoretical calculations

Calculations were performed by GaussView 5.0.9 [29] and Gaussian 09 AS64L-G09RevD.01 [30] programs. *Hartree-Fock* (HF) method was thus adopted with a mix basis set. At this stage, LANL2DZ was used for metal atoms and 6-31G(d) was used for the remaining atoms. Additionally, related electronic structure descriptors were calculated by using Eqs. (1)–(5).

$$I = -E_{SOMO} \tag{1}$$

$$A = -E_{LUMO} \tag{2}$$

$$E_{GAP} = E_{LUMO} - E_{SOMO} \tag{3}$$

$$\eta = \frac{I - A}{2} = \frac{E_{LUMO} - E_{SOMO}}{2} \tag{4}$$

$$\sigma = \frac{1}{\eta} \tag{5}$$

2.5. Biological tests

Antimicrobial tests were carried out using bacteria and fungi obtained from clinical samples. The microorganisms were *Staphylococcus aureus*, *Escherichia coli*, *Candida specie* and *Aspergillus niger*. The method by which these organisms were obtained was by plating out on selected solid medium; a small quantity of the samples from infected patient was streaked out on the selected medium, i.e. mantol salt, tosine methylene, blue agar and Sabouraud dextrose agar. These isolates were sub-cultured into nutrient agar and Sabouraud dextrose agar for bacteria and fungi, respectively. Then, 0.5 mL of each bacteria and fungi isolates were used to inoculate the medium based on the number of metal complexes to be tested. Holes of 6 mm diameter were bored on the seeded Mueller Hinton agar plates based on the number of the complexes fractions. Each hole was filled with a metal complex fraction: two concentrations were considered C_1 = 10 mg·mL^{-1} and C_2 = 20 mg·mL^{-1}. Plates were then incubated at 37 °C overnight and the zones around each disc were measured with a ruler.

3. Results and discussion

3.1. X-ray crystallographic study

3.1.1. Crystal structures description

The asymmetric unit of (**1**) consists of a discrete copper complex in which the metallic center is linked to three imidazole ligands through the three (N1A, N1B, N1C) nitrogen atoms and to a dihydrogencitrate anion acting as a bidentate ligand through

two oxygen donors: O6 belonging to the deprotonated α-carboxylato group and the hydroxyl oxygen O7, thus building a five-membered chelating ring (Fig. 1).

In order to describe the geometry of pentacoordinate complexes, the distortion parameter τ is calculated according to the equation $\tau = (\beta - \alpha)/60$, where α and β are the two largest angles measured around the metal center. Therefore, an ideal square pyramid corresponds to a τ value of 0, while τ = 1 in a perfect trigonal bipyramidal geometry [31]. From the values of α and β in (**1**) (148.09(5) and 169.39(5)°, respectively), it follows that τ = 0.355. This suggests that the Cu(II) ion in (**1**) adopts a geometry significantly distorted towards square pyramidal, with a N_3O_2 donor set in which the equatorial plane is occupied by the two citrate oxygens O6 and O7, and the two N1B and N1C nitrogens, with Cu—O/N bond distances ranging from 1.9417(11) to 2.0563(11) Å. The third imidazole nitrogen N1A is found in the apical position, with a longer bond distance of 2.1839(14) Å. The copper is 0.33 Å above the N_2O_2 plane towards the axially-coordinated N1A imidazole nitrogen. The distances are in the normal ranges and are consistent with those reported in similar imidazole-containing pentacoordinated copper(II) carboxylate structures like $[Cu(Im)_2(mal)]_n$ [32], $[Cu(H_2lac)_2(Im)]$, $[Cu(H_2mlac)_2(Im)]$ [33] and $[Cu(pydc)(H_2O)(4\text{-}mIm)_2].H_2O$ [34], where (Im, H_2mal, H_2lac, H_2mlac, H_2pydc, mIm) stands respectively for (imidazole, malonic acid, lactic acid, 2-methyllactic acid, pyridine-2,5-dicarboxylic acid, 4-methylimidazole). Summary of relevant bond lengths and angles is given in (Table 1).

The asymmetric unit of (**2**) consists of a mononuclear five-coordinated anionic copper(II) complex and a non-coordinating imidazolium cation (see Fig. 2). The crystal structure reveals that the metallic center is surrounded by two imidazole N1A and N1B nitrogen atoms and three oxygen donors of a tridentate hydrogencitrate ligand: O1 belonging to one of the two deprotonated β-carboxylic groups, O7 which originates from the hydroxyl group and O6 arising from the α-carboxylate group. It should be mentioned that the Cu(II) ion builds a seven-membered ring in addition to the edge-fused five-membered and six-membered chelating rings with the hydrogencitrate ligand.

By considering the two largest coordination angles within (**2**) (α = 166.84(6) and β = 169.79(6)°), the geometry around the copper(II) ion is best described as square pyramidal with a very small trigonal bipyramidal component (τ = 0.049). N1A, N1B, O6 and O7 define the equatorial positions, with Cu—O and Cu—N distances in the ranges 1.9474(12)–2.0088(10) Å and 1.9657(14)–1.9816(14) Å, respectively. The axial position is occupied by the third O1 hydrogencitrate oxygen, with a Cu—O bond distance of 2.3082(13) Å. The copper(II) ion is 0.146 Å above the N_2O_2 plane towards the axially-coordinated hydrogencitrate oxygen O1. The selected bond lengths and angles, listed in Table 1, are in agreement with the geometric parameters observed in other analogous imidazole complexes [35] and similar metallic citrate systems [36]. Furthermore, the imidazolium moiety shows geometric parameters comparing well with the values described in other imidazolium containing salts, like imidazolium fumarate [37], imidazolium 4-nitrophenolate 4-nitrophenol monohydrate [38], imidazolium 3-carboxy-4-hydroxybenzenesulfonate [39], imidazolium 2,4-dihydroxybenzoate [40] and 2-methylimidazolium hydrogen maleate [41]. It is worth to be noted that only two discretely mononuclear mixed-ligand copper (II) complexes based on citrate have been yet reported, namely ammonium bis[*citrato*(3-)]cuprate(II) [42] and tetraguanidinium

Table 1
Selected bond distances and angles in (**1**) and (**2**).

	Complex (**1**)	Complex (**2**)
Bond lengths (Å)		
Cu1—O1	–	2.3082 (13)
Cu1—O6	1.9417 (11)	1.9474 (12)
Cu1—O7	2.0563 (11)	2.0088 (10)
Cu1—N1A	2.1839 (14)	1.9816 (14)
Cu1—N1B	2.0170 (13)	1.9657 (14)
Cu1—N1C	1.9842 (13)	–
Bond angles (°)		
O1—Cu1—O7	–	82.59 (4)
O6—Cu1—O1	–	90.15 (5)
O6—Cu1—O7	78.39 (4)	81.20 (4)
O6—Cu1—N1A	91.08 (5)	87.28 (5)
O6—Cu1—N1B	89.59 (5)	169.79 (6)
O6—Cu1—N1C	169.39 (5)	–
N1A—Cu1—O1	–	103.90 (6)
N1A—Cu1—O7	104.05 (5)	166.84 (6)
N1B—Cu1—O1	–	98.79 (6)
N1B—Cu1—O7	148.09 (5)	95.01 (5)
N1B—Cu1—N1A	105.63 (6)	95.27 (6)
N1C—Cu1—O7	92.54 (5)	–
N1C—Cu1—N1A	96.50 (6)	–
N1C—Cu1—N1B	95.47 (6)	–

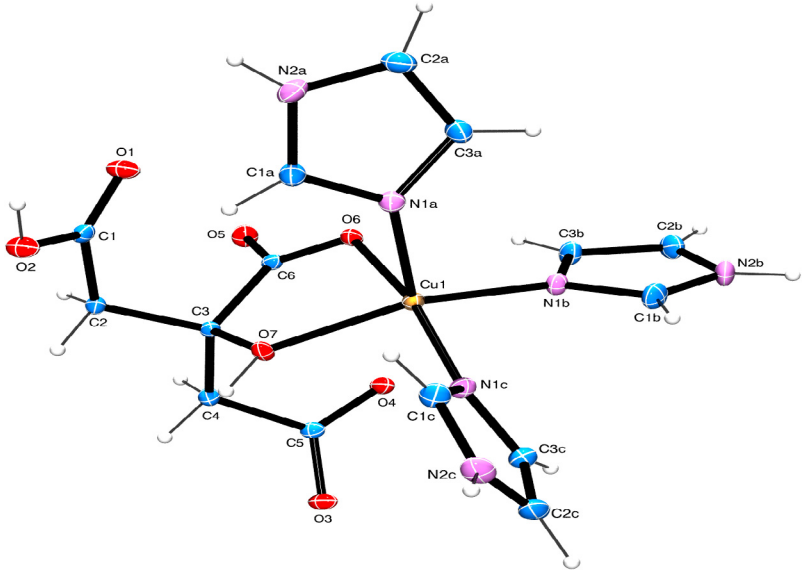

Fig. 1. A view of the asymmetric unit of (**1**) showing the atom-numbering scheme and thermal displacement ellipsoids drawn at the 30% probability level.

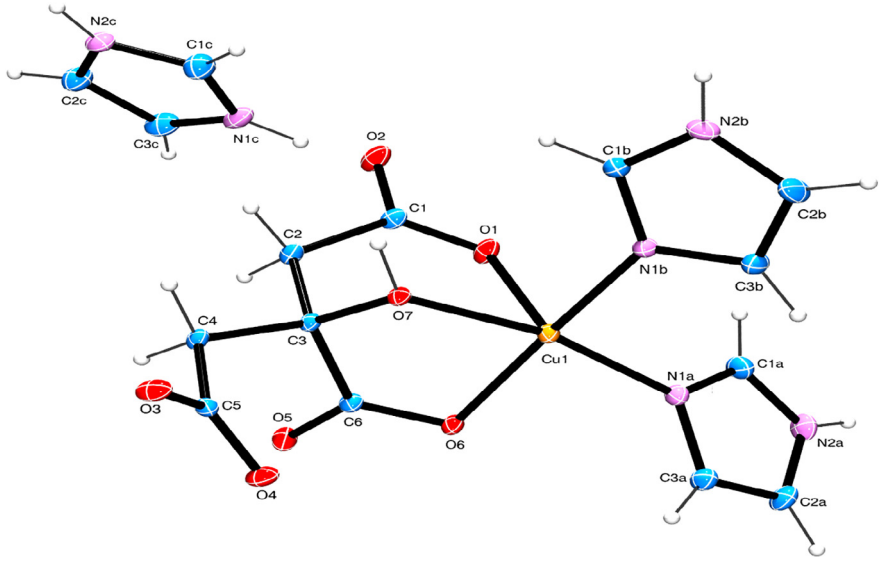

Fig. 2. A view of the asymmetric unit of (**2**) showing the atom-numbering scheme and thermal displacement ellipsoids drawn at the 30% probability level.

bis[*citrato*(3-)]-cuprate(II) dihydrate [43]. In both cases, the copper (II) ion is coordinated in an octahedral geometry to two centrosymmetrically related tridentate citrato(3-) ligands through the hydroxyl oxygen [2.341(3) and 2.2016 (7) Å, respectively] and the two oxygen atoms belonging to the α- and β-carboxylate groups [(1.977(3), 1.969(3) Å in the ammonium complex) and (1.9169 (7), 2.0857 (8) Å in the guanidinium complex)]. Moreover, four ammonium and four guanidinium cations come neutralizing the charge within the two complexes, respectively.

The crystal structures of the two complexes are mainly dominated by supramolecular N—H···O hydrogen-bonding (Table 2). Each molecule of (**1**) is thus surrounded by seven other complex molecules (Fig. 3a), bounded through four N—H···O intermolecular H-bonds. Among these, a chelated interaction involving the bifurcated imidazole N2B donor with the two deprotonated α-carboxylate O5 and O6 oxygens of the same citrate is observed [N2B—H2NB···O5, 3.060(2) Å, (x+½, $-y$+½, z+½) and N2B—H2NB···O6, 2.878(2) Å, (x+½, $-y$+½, z+½)]. These two interactions combine along the c-direction to build up infinite C(6) chains [44] connected together by means of the O7—H7···O3 hydrogen bond to produce bidimensional sheets in the (*bc*) plane. In addition, two moderate O—H···O hydrogen bonds result from the interaction of the bifurcated deprotonated β-carboxylate O3 acceptor with the hydroxyl O7 oxygen [O7—H7···O3, 2.586(1) Å, ($-x$+2, $-y$, $-z$ + 2)] and the protonated β-carboxyl O2 atom [O2—H2···O3, 2.689(2) Å, (x−1, y, z)]. It is worth to be mentioned that the O7—H7···O3 hydrogen bond delineates a symmetric $R_2^2(12)$ ring motif. The three-dimensional hydrogen-bonding framework also displays the contribution of four weak C—H···O and C—H···N interactions. These connect the citrate *C*2 atom with the β-carboxyl O2 oxygen, and a carbon of each

Table 2
Hydrogen bonds geometry (Å, °) in (**1**) and (**2**).

D—H···*A*	*D*—H	H···*A*	*D*···*A*	*D*—H···*A*
Complex (**1**)				
O2—H2···O3^{i}	0.82	1.90	2.689 (2)	161
C2—H2*D*···O1^{ii}	0.97	2.49	3.452 (2)	171
N2*A*—H2*NA*···O4^{i}	0.86	1.97	2.800 (2)	161
N2*C*—H2*NC*···O4^{iii}	0.86	2.05	2.868 (2)	158
C1*A*—H1*A*···O2^{iv}	0.93	2.62	3.414 (2)	144
N2*B*—H2*NB*···O6^{v}	0.86	2.16	2.878 (2)	141
N2*B*—H2*NB*···O5^{v}	0.86	2.26	3.060 (2)	155
C2*C*—H2*C*···O1^{vi}	0.93	2.56	3.276 (2)	134
C2*B*—H2*B*···N1*A*^{vii}	0.93	2.70	3.564 (3)	155
O7—H7···O3^{viii}	0.89	1.70	2.586 (1)	171
Complex (**2**)				
N2*A*—H2*NA*···O2^{iv}	0.86	1.92	2.778 (2)	172
N2*B*—H2*NB*···O4^{i}	0.86	1.89	2.735 (2)	166
C1*B*—H1*B*···O3^{ix}	0.93	2.39	3.172 (2)	142
C3*A*—H3*A*···O4^{x}	0.93	2.47	3.388 (2)	168
C2*B*—H2*B*···O4^{ii}	0.93	2.45	3.362 (2)	167
*C*2—H2*D*···O3^{ix}	0.97	2.58	3.123 (2)	116
N1*C*—H1*NC*···O2	0.86	1.82	2.678 (2)	180
N2*C*—H2*NC*···O6^{xi}	0.86	2.62	3.146 (2)	121
N2*C*—H2*NC*···O5^{xi}	0.86	1.84	2.680 (2)	164
C3*C*—H3*C*···O1^{xii}	0.93	2.34	3.222 (2)	159
O7—H7···O3^{ix}	0.88	1.63	2.516 (2)	175

Symmetry codes: (i) $x-1, y, z$; (ii) $-x+1, -y, -z+1$; (iii) $x, y, z+1$; (iv) $-x+1, -y, -z+2$; (v) $x+1/2, -y+1/2, z+1/2$; (vi) $x+1, y, z+1$; (vii) $x+1/2, -y+1/2, z-1/2$; (viii) $-x+2, -y, -z+2$; (ix) $-x+1, -y+1, -z+1$; (x) $-x+2, -y, -z+1$; (xi) $x-1, y+1, z$; (xii) $-x+1, -y, -z+2$.

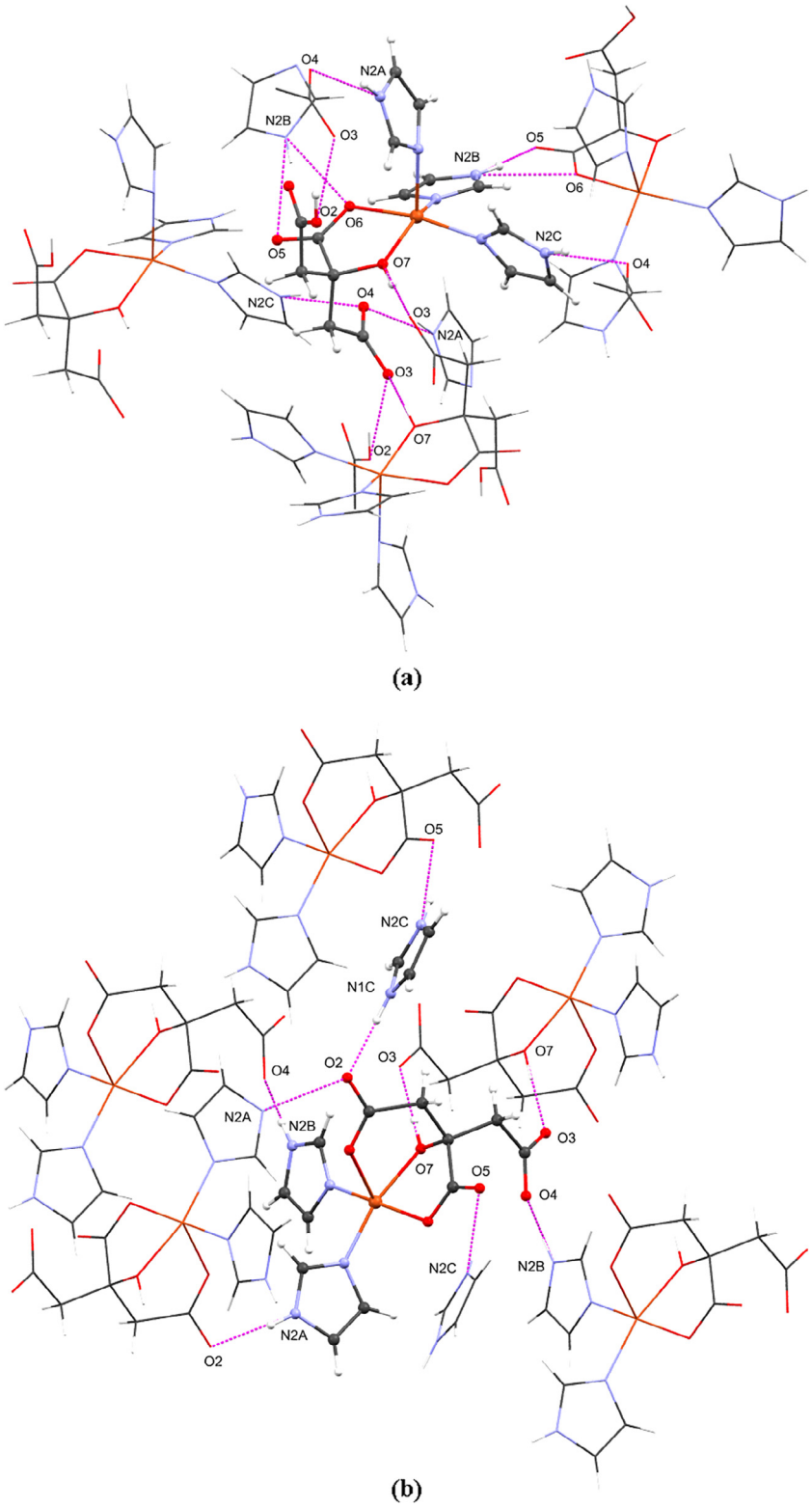

Fig. 3. A perspective view of the crystal structure of (a) (**1**) and (b) (**2**), highlighting the network of hydrogen bonds.

of the three imidazoles (C1A, C2B, C2C) with the protonated carboxyl O2 atom, the imidazole N1A nitrogen and the protonated β-carboxyl O1 oxygen, respectively.

Each anionic copper complex in compound (**2**) exhibits four complex neighbors and two uncoordinated imidazolium cations in its immediate surroundings. Conversely, each free imidazolium moiety interacts with two copper complexes (Fig. 3b). The complex anion is linked to the four neighboring complexes through two moderate N—H···O hydrogen bonds (and their reciprocal O···H—N interactions). These involve the two N2A and N2B nitrogen atoms and the two β-carboxylate O2 and O4 oxygens [N2A—H2NA···O2, 2.778(2) Å, (−*x*+1, −*y*, −*z*+2); N2B—H2NB···O4, 2.735(2) Å, (*x*−1,

y, *z*)]. This connection is as well reinforced *via* two O–H···O hydrogen bonds involving the hydroxyl O7 oxygen and the β-carboxylate O3 atom [O7—H7···O3, 2.516(2) Å, (−*x*+1, −*y*+1, −*z*+1)], which combine together, as in (**1**), to build dimeric complex moieties described as $R_2^2(12)$ graph-set rings. H-bonding resulting from the interaction between each complex molecule with imidazolium cations involves β-carboxylate O2 oxygen, which interacts with imidazolium N1C atom. Additionally, the α-carboxylate group (O5 and O6) is engaged in a chelate bond with the imidazolium N2C nitrogen, resulting in one moderate and one weak N—H···O hydrogen bond (Table 2). Compound (**2**) shows infinite chains of complex molecules stabilized basically by the N2B—H2NB···O4 interaction which define a C(10) descriptor [44]. These chains are further linked together by means of N2A—H2NA···O2 and O7—H7···O3 to yield infinite sheets parallel to the (*ac*) plane. Similarly to (**1**), weak C—H···O intermolecular forces contribute to stabilize the three-dimensional hydrogen-bonding networks in (**2**); however no C—H···N interactions have been observed.

3.1.2. Hirshfeld surface analysis

Hirshfeld surface analysis [45] represents an appealing approach to the investigation of the different contacts between molecules in crystals. It has proven to be a useful tool for the analysis and visualization of intermolecular interactions and therefore of the crystal packing behavior of molecules, in particular with the purpose of making structural comparisons between compounds. It is furthermore of interest to analyze the intermolecular interactions present in the crystal packing in terms of a bi-dimensional visualization of d_e and d_i based on decomposition of the *Hirshfeld* surfaces into contributions from the different contacts and generated as a 2D-fingerprint plot [46]. The different properties mapped on the *Hirshfeld* surfaces and the fingerprint plots were generated using *CrystalExplorer* 3.1 [47]. The relative contributions of the different interactions of compounds (**1**) and (**2**) to the global *Hirshfeld* surfaces (Scheme 1) are given as full and decomposed 2D-finger plots, and are illustrated in Figs. 4 and S3, respectively.

The fingerprints of both compounds exhibit contribution similarity of the different intermolecular contacts except for the O···H/H···O contacts. These are considered as dominant and appear as a pair of sharp symmetric spikes (Figs. S3a and S3b), which are more significant over the total *Hirshfeld* surface around (**2**) (45.4%) compared to (**1**) (37.8%). Nevertheless, in both compounds these contacts could be attributed to the intermolecular O—H···O, N—H···O and C—H···O hydrogen-bonding interactions, and show prominent long spikes at $d_e + d_i = 1.6$ Å in (**1**) and at $d_e + d_i = 1.55$ Å in (**2**), resulting from the strong reciprocal interactions O7—H7···O3/O3···H7—O7. This is reflected by the presence of the two large red spots over the d_{norm} surface defined by features (1) and (9) in Figs. S4a and S4b, whereas the small red dots (features (8) for compound (**1**) in (Fig. S4a)) represent the weak C—H···O/O···H—C hydrogen bonds, considering that the spot size and color depends on the interaction strength. The scattered points covering a large region of the two-dimensional maps (Figs. S3c and S3d) arise from the H···H contacts and are observed to be the second highest contributor towards the total *Hirshfeld* areas, with a contribution of 37.5% and 31.3% for (**1**) *vs.* (**2**). As it can be seen from the two figures, the shortest contacts observed at about $d_e = d_i \sim 1.19$ Å in (**1**) and $d_e = d_i \sim 1.08$ Å in (**2**) are associated to the non-classical interactions *C*2—H2E···H1A—C1A and C4—H4A···H1A—C1A, respectively. The C···H/H···C contacts appearing as wings in the 2D-histograms (Figs. S3e and S3f) are less significant and represent 15.7% and 11.3% from the whole histograms of (**1**) and (**2**), respectively. The two wings show limits at $d_e + d_i \sim 2.62$ Å and $d_e + d_i \sim 2.54$ Å resulting from shortest contacts which could be related to N—H···π and C—H···π interactions, respectively, involving the imidazole (N2B, C1A) atoms in (**1**) and (C1A, C3C) carbons in (**2**). Moreover, there are 7.1% and 5.9% participations to the global areas of (**1**) and (**2**) coming from the N···H/H···N contacts (Figs. S3g and S3h), with two shortest interactions; namely C2B—H2B···N2A and C2C—H2C···N2A appearing at $d_e + d_i \sim 2.55$ Å and ~2.68 Å, respectively. A final observation deriving from our description based on fingerprint plots concerns the relative areas associated with the C···C and N···C/C···N contacts given in Figs. S5a and S5b and related with the planar π···π stacking arrangement and *lp*···π/π···*lp* interactions in compound (**2**). In fact from the two Figures, it can be seen that less than 3% of the surface is identified as N···C/C···N contacts, whereas the C···C forces are less frequent with around 2% of the entire molecular surface. These numbers are supported by the appearance of red and blue triangles on the shape-indexed surface of (**2**), as indicated by black arrows in Fig. S6. It is worth to be noted that this is compensated in (**1**) by the observation of around 2% of the total *Hirshfeld* area, resulting equally from the contribution of O···O and O···C/C···O contacts which are associated to the presence of *lp*···*lp* and *lp*···π/π···*lp* interactions.

In addition, the *Hirshfeld* surfaces associated to compounds (**1**) and (**2**) have been displayed with the *MoProViewer* software [48] and colored according to the values of the atomic number of the atoms contributing most to the local electron density (Fig. 5b and e), in order to highlight the chemical type of the closest interacting atoms in the crystal surrounding (Fig. 5c and f).

3.1.3. Enrichment ratio

The intermolecular interactions in (**1**) and (**2**) were further evaluated by computing the enrichment ratios (*E*) [49], in order to examine the likelihood of two chemical species in the two complexes to be in contact and therefore to form intermolecular interactions with themselves and with the other species. The proportion of actual contacts in the crystal structures of (**1**) and (**2**), the theoretical proportion of random contacts and the related enrichment ratios are given in Table 3.

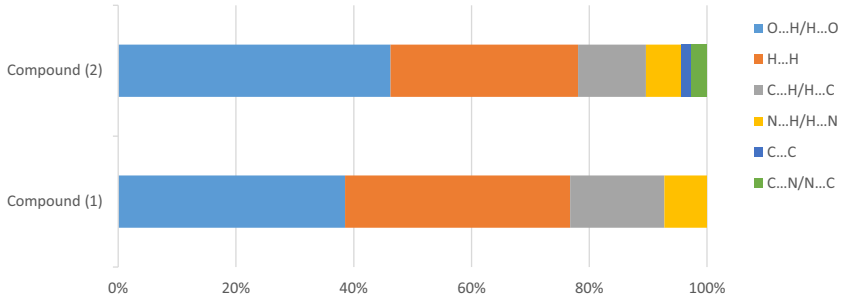

Scheme 1. Relative contributions of intermolecular contacts to the *Hirshfeld* areas in (**1**) and (**2**).

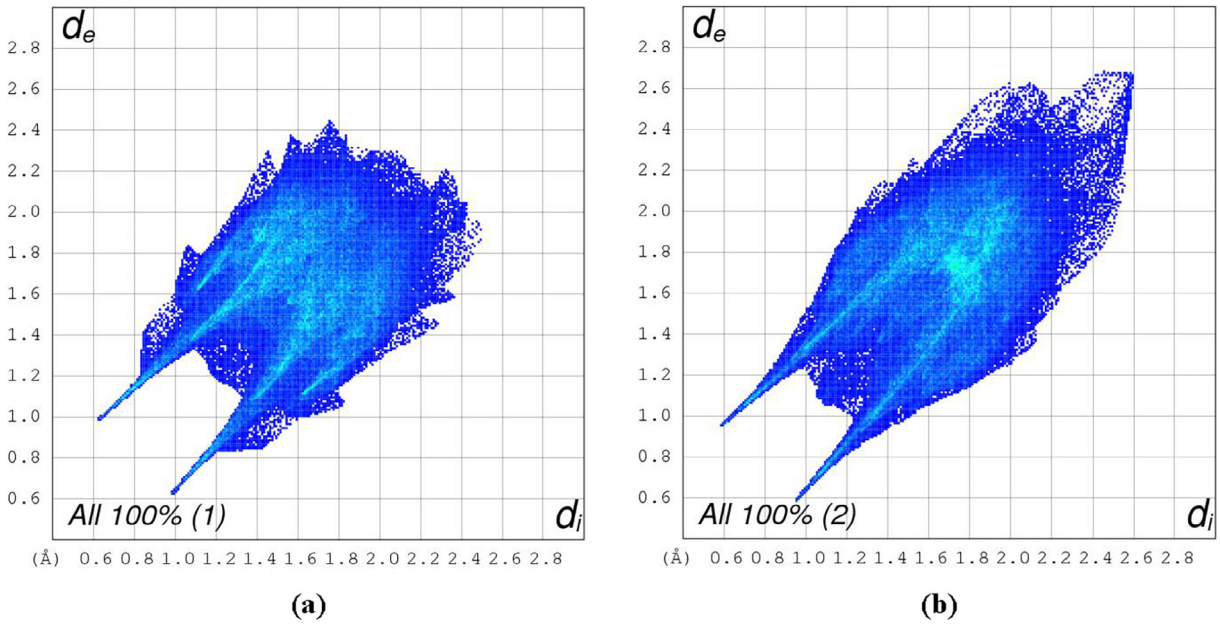

Fig. 4. Full 2D-fingerprint plots in (a) (**1**) and (b) (**2**).

For pairs of elements with a high propensity to form contacts the enrichment ratio is larger than unity, while values lower than unity are found for pairs tending to avoid contacts. Therefore, the H···H contacts in the two compounds are slightly under-represented with an enrichment ratio E_{HH} of about 0.80 in both cases. Though, being enriched with $E_{HO} = 1.58$ the O—H···O, N—H···O and C—H···O hydrogen bonds appear to be the driving forces in the crystal packing of (**2**) compared to (**1**), which shows a lower enrichment of 1.37. On the other hand, the H···N and H···C contacts are over-represented in (**1**) in comparison to (**2**) with $E_{HN/C}$ values of 1.45 and 1.39 respectively (*vs.* ∼1 in the case of (**2**)), thus showing a high propensity to form C—H···N, C—H···π and related interactions, as proved by means of the *Hirshfeld* surface analysis. It is to be noted that the formation of extensive π···*lp* interactions in (**2**) is reflected in the relatively high value of E_{CN} being equal to 2.89, while the propensity of such interactions in (**1**) is absolutely insignificant. The C···O and O···O contacts are in the two cases very impoverished, with $E_{OC/O}$ less than 0.3 in (**1**) and 0.02 in (**2**). Moreover, the other XY contacts and self-contacts involving nitrogen, carbon and copper are completely avoided. Fig. S7 presents the *Hirshfeld* surfaces built around (**1**) and (**2**), and displayed according to the different contact types and their proportions.

3.1.4. Topological analysis

Topological description of the crystal structures could be undertaken by finding simple net models [50] that usually ignore the geometrical parameters of an atomic array and rather focus on the overall structure connectivity [51]. For this purpose and according to a topological analysis using *ToposPro* program [52], the three-dimensional hydrogen-bonding frameworks observed in (**1**) and (**2**) could be described as simplified nodal nets. Consequently, the entire assembly of (**1**) can be simplified to a **sev** (*sqc*44) uninodal (7)-connected underlying net (Fig. S8) having the Schläfli symbol $\{4^{17}.6^4\}$. Here, the nodes are the mass centers of the copper complex molecules and the connections between them are made of edges that mimic the hydrogen-bonding patterns made of two O—H···O and four N—H···O interactions.

From a topological point of view, the copper complex molecules in (**2**) serve as 6-coordinated nodes, bonded to four other complex molecules and two free imidazole moieties (Fig. S9c). The imidazolium cations could be represented as 2-connected nodes which guarantee the link between two different complex molecules by means of two N—H···O interactions. The two types of nodes are further interconnected through edges built of the different H-bonds present in the crystal structure, and the resulting 3D-framework is thus a (2,6)-connected binodal net with a unique $\{4^4.6^{10}.10\}\{6\}$ topology. If we consider that the bridging imidazolium cations (2-coordinated purple nodes) could be merged to the 6-connected nodes (yellow nodes) and contracted to edges, then a secondary simplification should be additionally applied to obtain the standard representation. Therefore, the previously obtained network could simplify further to a 6-connected uninodal primitive cubic lattice **pcu** (*sqc*1) underlying net with a point symbol of $\{4^{12}.6^3\}$ (Fig. S10).

3.2. Computational results

3.2.1. Optimized structures

The quantum HF computational analysis was performed to gain a better insight into the electronic and vibrational properties of the two mixed-ligand copper(II) complexes. Calculated structures of the complexes are represented in Figs. S11a and S11b. Some relevant theoretical structural parameters obtained at HF/6-31G(d) (LANL2DZ) level in the gas phase are compared to the experimental ones in Table 4.

As it can be noticed from Table 4, the calculated bond lengths and bond angles in complexes (**1**) and (**2**) are approximately similar to the experimental values obtained by X-ray crystallography, suggesting a square pyramidal geometry for the two structures with τ values of 0.216 and 0.095, respectively. However, a slight deviation has been observed especially in the (Cu1—N1B, Cu1—O7) bonds of (**1**) and the (Cu1—O1, Cu1—O7) bonds of (**2**), making the apical position occupied by O7 in the two cases instead of N1A and O1.

3.2.2. Spectral analysis

The calculated IR spectra of both compounds were obtained at HF/6-31G(d)(LANL2DZ) level in the gas phase and are depicted in Figs. S12a and S12b. Some stretching frequencies given in Table 5 are very comparable in both complexes, such as the stretching

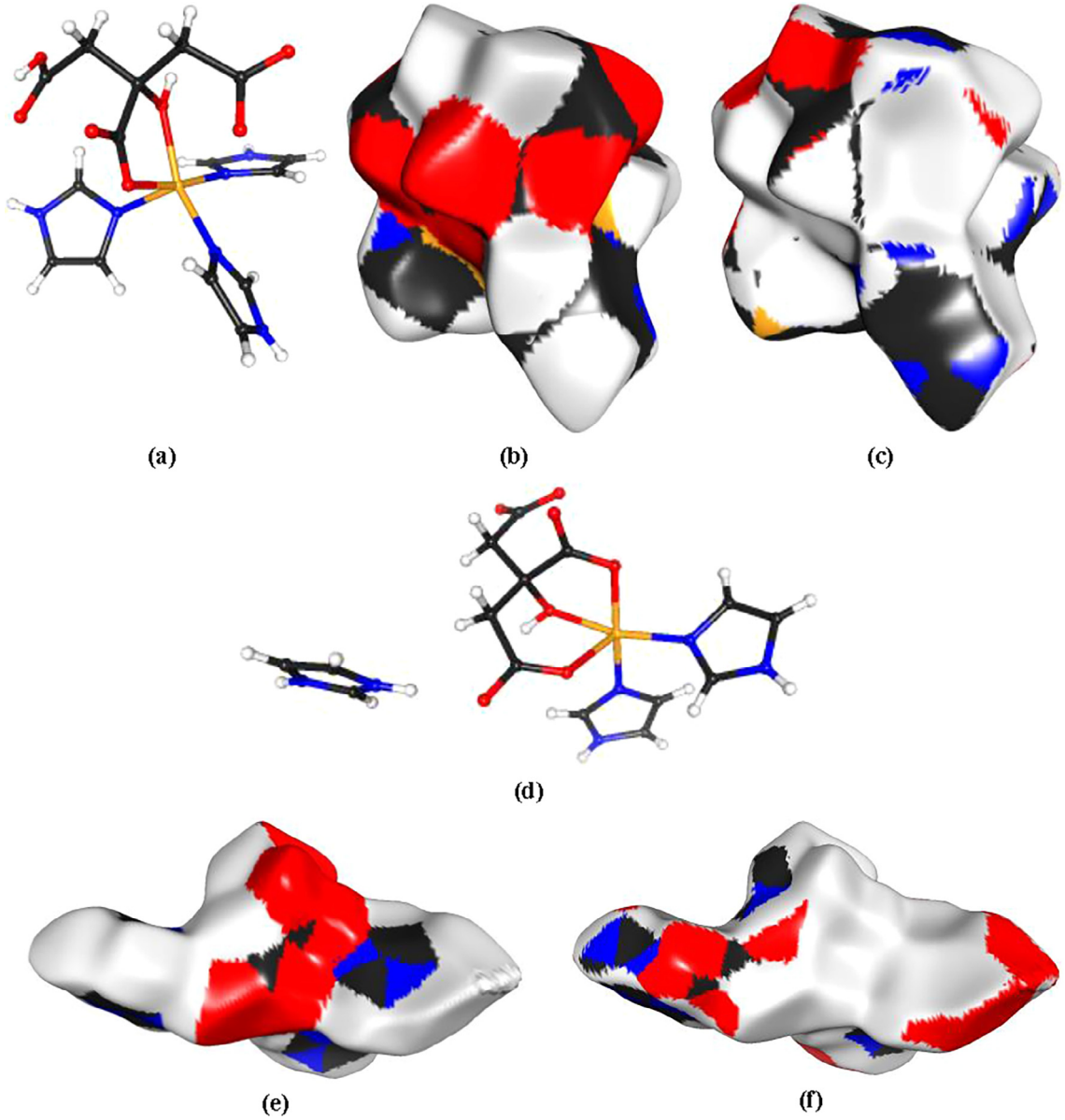

Fig. 5. (a), (d) Orientation of the molecules of (**1**) and (**2**). *Hirshfeld* surfaces around the asymmetric units of (**1**) and (**2**) colored according to the (b), (e) internal or (c), (f) external atoms contributing most to the electron density.

vibration modes of the O—H and N—H bonds around 4000 cm^{-1} and 3900 cm^{-1}, respectively.

3.2.3. Electronic structure descriptors

The chemical reactivity of the studied copper complexes was ranked by calculating the electronic descriptors of their molecular structures. Thus, the energy of singly occupied molecular orbital (E_{SOMO}), the energy of the lowest unoccupied molecular orbital (E_{LUMO}), the energy gap (E_{GAP}), the chemical hardness (η), the chemical softness (σ), the dipole moment (μ), the polarizability (α) and the hyperpolarizability (β) were calculated by using Eqs. (1)–(5) and their values are given in Table 6.

Chemical reactivity increases with the increase of E_{SOMO}, σ, μ, α and β. As a result, chemical reactivity ranking should be as follow:

Complex (**2**) > Complex (**1**) (in E_{SOMO}, σ, μ and β)
Complex (**1**) > Complex (**2**) (in α)

On the other hand, the chemical reactivity increases with decreasing E_{LUMO}, E_{GAP} and η. According to these parameters, the chemical reactivity ranking should be as follow:

Complex (**2**) > Complex (**1**) (in E_{GAP} and η)
Complex (**1**) > Complex (**2**) (in E_{LUMO})

And thus, complex (**2**) is more reactive than complex (**1**).

3.3. Spectroscopic IR study

The FT-IR spectra of the two complexes are illustrated in Figs. S13a and S13b. The vibrational assignments have been made by comparison with the assignments reported earlier for similar imidazole and citrate systems, as well as with the calculated spectra. Similarly to other citrate-complexes [53], the stretching frequency ν(O—H) of the citrate hydroxyl group occurs as a strong

Table 3
Percentages of *Hirshfeld* surface contacts, derived random contacts and enrichment ratios for the different chemical species in (**1**) and (**2**).

	(**1**)					(**2**)				
	H	O	N	C	Cu	H	O	N	C	Cu
Contacts (C, %)[a]										
H	37.5	–	–	–	–	31.3	–	–	–	–
O	37.8	0.9	–	–	–	45.4	0.1	–	–	–
N	7.1	0.0	0.0	–	–	5.9	0.0	0.5	–	–
C	15.7	0.9	0.0	0.0	–	11.3	0.1	2.6	1.7	–
Cu	0.0	0.0	0.0	0.0	0.0	0.5	0.0	0.0	0.7	0.0
Surface (S, %)										
	67.8	20.3	3.6	8.3	0.0	62.9	22.9	4.8	9.1	0.6
Random contacts (R, %)										
H	46.0	–	–	–	–	39.6	–	–	–	–
O	27.5	4.1	–	–	–	28.8	5.2	–	–	–
N	4.9	1.5	0.1	–	–	6.0	2.2	0.2	–	–
C	11.3	3.4	0.6	0.7	–	11.4	4.2	0.9	0.8	–
Cu	0.0	0.0	0.0	0.0	0.0	0.8	0.3	0.1	0.1	0.0
Enrichment (E)[b]										
H	0.82	–	–	–	–	0.80	–	–	–	–
O	1.37	0.22	–	–	–	1.58	0.02	–	–	–
N	1.45	0.00	–	–	–	0.98	0.0	–	–	–
C	1.39	0.26	–	–	–	0.99	0.02	2.89	–	–
Cu	–	–	–	–	–	–	–	–	–	–

[a] The contacts proportions are obtained from the *CrystalExplorer* software [47].
[b] The enrichment ratios are not computed for the random contacts lower than 0.9% as they are not meaningful [49].

Table 4
Comparative experimental and calculated structural parameters of the two copper complexes.

	Bond Lengths (Å)			Bond Angles (°)	
	Experimental	Calculated		Experimental	Calculated
*For Complex (**1**)*					
Cu1—N1A	2.184	2.149	N1A—Cu1—N1B	105.6	103.8
Cu1—N1B	2.017	2.304	N1A—Cu1—N1C	96.5	90.8
Cu1—N1C	1.984	2.149	N1A—Cu1—O6	91.1	87.8
Cu1—O6	1.942	1.946	N1A—Cu1—O7	104.1	97.7
Cu1—O7	2.056	2.643	N1B—Cu1—N1C	95.5	96.3
–	–	–	N1B—Cu1—O6	89.6	96.1
–	–	–	N1B—Cu1—O7	148.1	154.5
–	–	–	N1C—Cu1—O6	169.4	167.5
–	–	–	N1C—Cu1—O7	92.5	96.8
–	–	–	O6—Cu1—O7	78.4	71.1
*For Complex (**2**)*					
Cu1—N1A	1.982	2.153	N1A—Cu1—N1B	95.3	92.8
Cu1—N1B	1.966	2.141	N1A—Cu1—O1	103.9	176
Cu1—O1	2.308	1.946	N1A—Cu1—O6	87.28	87.1
Cu1—O6	1.947	1.929	N1A—Cu1—O7	166.8	93.5
Cu1—O7	2.009	2.388	N1B—Cu1—O1	98.8	84.8
–	–	–	N1B—Cu1—O6	169.8	170.3
–	–	–	N1B—Cu1—O7	95	112.5
–	–	–	O1—Cu1—O6	90.2	95.6
–	–	–	O1—Cu1—O7	82.6	85
–	–	–	O6—Cu1—O7	81.2	77.1

Table 5
Stretching vibrations and related frequencies (cm^{-1}) in the calculated IR spectra of the complexes.

Vibration mode	Frequency	
	Complex (**1**)	Complex (**2**)
ν_{OH}	4047	4070
ν_{NH}	3911	3914
$\nu_{CHAromatic}$	3492	3488
$\nu_{CHAliphatic}$	3182	3158
$\nu_{C=O}$	1938	1909
ν_{C-C}, $\nu_{C=O}$	1512	1544

broad band near 3157 cm^{-1} for complex (**1**). In complex (**2**) it is sharper and appears at 3150 cm^{-1}. Additionally, the ν(O—H) vibration of the protonated carboxyl moiety in (**1**) overlaps with the former frequency range. Furthermore, the experimental/calculated antisymmetric ν_{as}(—CO_2) and the symmetric ν_s(—CO_2) carboxylate stretching vibrations for the coordinated citrate occur at 1647/1938 and 1419/1512 cm^{-1} in (**1**) and at 1591/1909 and 1381/1544 cm^{-1} in (**2**). The positions of these carboxylate stretching vibrations are within the range expected for carboxylate groups [54] and are shifted to lower frequencies compared to free citric acid [55], denoting changes in vibrational status upon complexation to copper. In the IR spectrum of (**1**) there is a strong sharp absorption band at 1735 cm^{-1} characteristic of the $\nu(CO_2H)$ stretching. This vibration mainly results from the uncoordinated β-carboxylic acid group (1720 cm^{-1} in Ref. [56]) and is absent in the spectrum of (**2**), confirming complete deprotonation of its three carboxylic acid groups. In addition, sharp-to-medium bands at 523, 599 and 670 cm^{-1} are mainly generated by the (—CO_2) rocking,

Table 6
Calculated electronic structure descriptors for the two studied complexes.

	E^1_{SOMO}	E^1_{LUMO}	I^1	A^1	E^1_{GAP}
Complex (**1**)	−8.857	3.088	8.857	−3.088	11.945
Complex (**2**)	−4.611	4.311	4.611	−4.311	8.922
	η^1	**σ^2**	**μ^3**	**α^4**	**β^4**
Complex (**1**)	5.972	0.167	12.955	189.785	106.681
Complex (**2**)	4.461	0.224	30.660	152.778	353.385

[1]in eV, [2]in eV^{-1}, [3]in Debye, [4]in a.u.

wagging and bending vibrations [57] in complex (**1**). The same vibration modes for (**2**) occur at about 537, 625 and 657 cm^{-1}. On the other hand, the two complexes exhibit infrared frequencies appearing as doublets at 3148, 3127 cm^{-1} for (**1**) and at 3137, 3117 cm^{-1} for (**2**), which are assigned to the ν(N—H) stretching bands of the coordinated imidazole ligands and the non-coordinated imidazolium moieties. These frequencies cover the same range as in related complexes based on imidazole [57] appearing in the region 3166–3155 cm^{-1}, and show bigger shifts of approximately 228, 249 cm^{-1} in (**1**) and 239, 259 cm^{-1} in (**2**) to lower frequencies compared to free imidazole [58], for only 221 and 210 cm^{-1} observed in ref 55. The observed shifting size reflects the strength of the hydrogen bonds resulting from the imidazole nitrogens. It is to be noted that the ν(O—H) and ν(N—H) stretching vibration values are found to be smaller than the calculated frequencies associated to the two studied complexes, with ($\Delta\nu_{O-H}$, $\Delta\nu_{N-H}$) being (890, 763–784 cm^{-1}) and (920, 777–797 cm^{-1}) in (**1**) and (**2**), respectively. This difference could be explained by the presence of O—H···O and N—H···O hydrogen bonds in the two crystal structures yielding a shift to the lower frequencies while the calculations were performed in the gas phase. It is worth noting that the medium broad bands appearing at around 3025–2971 and 3042–2937 cm^{-1} in complexes (**1**) and (**2**), respectively, are due to the ν(C—H) vibrations of the citrate and imidazole moieties, as reported in [55] and [59] (2994 and 3122–2973 cm^{-1}, respectively).

Moreover, the broad bands at 1571 and 1587 cm^{-1} in (**1**) and (**2**), respectively, are assigned to the (N—H) in-plane bending vibrations [59]. The same band lies at 1223 cm^{-1} in the free imidazole molecule [58]; the observed upward shift in (**1**) and (**2**) is likely due to the presence of strong and moderate intermolecular hydrogen bonds. Both spectra show the presence of ν(C=C) and ν(C=N) stretching vibrations in the region 1535–1495 cm^{-1} and 1491–1447 cm^{-1}, respectively [60]. The spectra also exhibit absorption bands at 1418, 1383, 1364, 941 cm^{-1} in (**1**) and at 1427, 1384, 1331, 959 cm^{-1} in (**2**) attributed to the citrate (–CH_2) bending, wagging, twisting and rocking deformation modes [57]. The (–CH) in-plane bending of the imidazole molecules occurs in the 1260–1128 cm^{-1} range for (**1**) and at 1263–1108 cm^{-1} for (**2**); the corresponding out-of-plane bending appears as a very strong sharp band at 1068 cm^{-1} in both complexes [57]. The bands at around 540/441 cm^{-1} for (**1**) and 584/432 cm^{-1} for (**2**) can be assigned to the ν(Cu—O) and ν(Cu—N) stretching vibrations [61].

3.4. Magnetic properties

The molar magnetic susceptibility of polycrystalline samples of (**1**) and (**2**) was measured in a magnetic field of 1 kOe and in the temperature range 2–300 K. Magnetic data showed that both compounds behave as paramagnets down to the lowest temperature explored, with Curie constants typical of copper(II) centers (ca. 0.4 emu K mol^{-1}) and no signs of intermolecular magnetic interactions.

3.5. Biological activity

Each complex was tested for its in vitro antibacterial activity against *Staphylococcus aureus* and *Escherichia coli* as examples of Gram-positive bacteria and Gram-negative bacteria, respectively. After plates' incubation, the zones of inhibition formed were measured and accumulated in Table 7. Furthermore, the same table presents the results of additional tests against two fungi, namely *Candida specie* and *Aspergillus niger*. Concentrations used were 10 mg·mL^{-1} (Concentration 1) and 20 mg·mL^{-1} (Concentration 2).

On the basis of the minimum inhibitory concentration (M.I.C) and the diameter of the inhibition zone, complex (**1**) showed higher fungicidal activity against *Aspergillus niger* (15 mm at 10 mg·mL^{-1}) compared to its inhibition of *Candida specie* (10 mm at 10 mg·mL^{-1}). The same behavior was observed for complex (**2**) but with higher response (20 mm at 10 mg·mL^{-1} for *Aspergillus niger vs.* 16 mm at 10 mg·mL^{-1} for *Candida specie*). Moreover, both complexes were found to have high activity against *Staphylococcus aureus* (15 mm for complex (**1**) and 18 mm for complex (**2**), at 10 mg·mL^{-1}). Significantly, antibacterial activity of complex (**1**) against *Escherichia coli* was observed to be significant (10 mm at 20 mg·mL^{-1}) compared to complex (**2**), which showed no effect on the same bacteria. The obtained results for both complexes are in agreement with the literature [62,63] assuming that the coordination of an organic ligand to a metallic center magnifies its antimicrobial activity due to the greater lipophilic nature of the complex. This improved lipophilicity enhances the penetration of the complexes into lipid membrane and inhibits the metal binding sites on enzymes of microorganisms. Complex (**2**) has the additional advantage of combining the free ligand and the coordinated-ligand molecule in its structure, resulting in a more potent antifungal and antibacterial activity compared to complex

Table 7
Diameter of the inhibition zone (mm) for the two complexes.

	Complex (**1**)		Complex (**2**)	
	C_1 = 10 mg·mL^{-1}	C_2 = 20 mg·mL^{-1}	C_1 = 10 mg·mL^{-1}	C_2 = 20 mg·mL^{-1}
Staphylococcus aureus	15	18	18	21
Escherichia coli	NE	10	NE	NE
Candida specie	10	13	16	21
Aspergillus niger	15	18	20	23

NE = No effect.

(**1**). Significantly, the calculated electronic structure descriptors indeed predict a greater chemical reactivity for (**2**) than for (**1**). It is to be noted that both complexes' activities are comparable to two other mixed-ligand imidazole-containing Cu(II) complexes based on two well-known broad spectrum antibacterial and synthetic chemotherapeutic agents, namely moxifloxacin hydrochloride [64] and pefloxacin [65]. The two resulting complexes, $[Cu(MOX)(HIm)Cl{\cdot}H_2O]_2{\cdot}2H_2O$ [66] and $[Cu(PEF)(HIm)Cl]{\cdot}2{\cdot}5H_2O$ [67] with (MOX = moxifloxacin and PEF = pefloxacin), were screened in vitro against *E. coli* and *S. aureus*, and have showed both an excellent activity. Similarly, $[Cu(HOr)(H_2O)_2(2\text{-meim})]$ with (HOr = orotate and 2-meim = 2-methylimidazole) [68] showed to be effective against *E. coli* and *S. aureus* with a MIC of 1800 $\mu g{\cdot}mL^{-1}$ (the complex has activity against *C. albicans* and *P. aeruginosa* as well). However, in the case of $[Cu(pydc)_2(H_2O)(4\text{-Meim})_2]{\cdot}H_2O$, with (pydc = pyridine-2,5-dicarboxylate and 4-Meim = 4-methylimidazole) [34], showed unclear zone against only *B. cereus* and *E. aerogenes* (clinic), and did not display any antibacterial or antifungal activity against the herein mentioned microorganisms and yeasts.

4. Conclusion

Two new concomitantly synthesized copper (II) complexes based on imidazole and citrate ligands were prepared, characterized by single-crystal X-ray diffraction and FTIR spectroscopy, and their magnetic and biological properties were studied. The crystallographic study revealed that the complexes are pentacoordinated and form extensive 3D propagating frameworks as a result of strong and moderate O—H···O and N—H···O hydrogen-bonding patterns. The *Hirshfeld* surface analysis indicated that the two crystal structures are dominated by the O···H/H···O, H···H and C···H/H···C non-covalent interactions. Moreover, the N···H/H···N contacts exhibit a high propensity to form C—H···N interactions. The C···O and O···O contacts are very impoverished, and the $\pi\cdots lp$ interactions in (**2**) are over-represented with E_{CN} being 2.89. The FTIR vibrational absorptions are in full agreement with the crystallographic data. In addition, computational investigations of the studied complexes were performed by using HF method with 6-31G(d)(LANL2DZ) mix basis sets in the gas phase. The geometric and spectral analyses showed an agreement with the experimental ones. Additionally, the chemical reactivity of the complexes was investigated by electronic structure descriptors, showing that complex (**2**) is more reactive than complex (**1**). Variable temperature magnetic studies down to 2 K indicated a paramagnetic behavior for both compounds, with no signs of intermolecular magnetic interactions through the extensive hydrogen-bonding network. The antimicrobial tests suggested that the two complexes are promising against *Staphylococcus aureus*, though only complex (**1**) was found to be effective against *Escherichia coli*. Furthermore, (**1**) and (**2**) showed significant fungicidal activity against *Aspergillus niger* and *Candida specie*. However, (**2**) displayed higher activity compared to (**1**), this behavior was predicted by exploring the computational chemical reactivity of the two complexes. In future stages of our investigation, we are planning to focus on the cytotoxic effect of the two newly synthesized imidazole complexes and the heteronuclear imidazole-based frameworks. Furthermore, the effect of the reaction temperature and the pH on the composition and the dimensionality of these systems will be performed.

Acknowledgements

The financial support from Université Abbes Laghrour Khenchela (Algeria), TUBITAK ULAKBIM, High Performance and Grid Computing Center (TRUBA Resources, Turkey), Spanish MINECO MAT2016-78155-C2-1-R, FPI grant BES-2011-046948 to MSM.A., Gobierno del Principado de Asturias (GRUPIN14-060) and FEDER are acknowledged. A. D. gratefully acknowledges Pr. A. Djelloul and Pr. A. Boumaza (University of Khenchela) for the FTIR measurements.

Appendix A. Supplementary data

Supplementary data associated with this article can be found, in the online version, at https://doi.org/10.1016/j.ica.2018.03.011.

References

[1] A. Bhatnagar, P.K. Sharma, N. Kumar, Int. J. Pharm. Tech. Res. 3 (1) (2011) 268–282.
[2] (a) T. Nakamura, H. Kakinuma, H. Umemiya, H. Amada, N. Miyata, K. Taniguchi, K. Bando, M. Sato, Bioorg. Med. Chem. Lett 14 (2004) 333–336;
(b) P.G. Nantermet, J.C. Barrow, S.R. Lindsley, M. Young, S. Mao, S. Carroll, C. Bailey, M. Bosserman, D. Colussi, D.R. McMasters, J.P. Vacca, H.G. Selnick, Bioorg. Med. Chem. Lett 14 (2004) 2141–2145;
(c) S. Emami, A. Foroumadi, M. Falahati, E. Lotfali, S. Rajabalian, S. Ahmed Ebrahimi, S. Farahyarc, A. Shafiee, Bioorg. Med. Chem. Lett 18 (2008) 141–146.
[3] M. Maru, M.K. Shah, J. Chem. Pharm. Res. 4 (3) (2012) 1638–1643.
[4] J. Reedijk, E. Bouwman, Bioinorganic Catalysis, Marcel Dekker Inc., New York & Basel, 1999.
[5] K.D. Karlin, Z. Tyeklar, Bioinorganic Chemistry of Copper, Chapman & Hall, New York, 1993.
[6] E. Colacio, M. Ghazi, R. Kivekäs, M. Klinga, F. Lloret, J.M. Moreno, Inorg Chem 39 (13) (2000) 2770–2776.
[7] M.T. Caudle, J.W. Kampf, M.L. Kirk, P.G. Rasmussen, V.L. Pecoraro, J. Am. Chem. Soc 119 (39) (1997) 9297–9298.
[8] (a) L. Casella, L. De Gioia, G.F. Silvestri, E. Monzani, C. Redaelli, R. Roncone, L. Santagostini, J. Inorg. Biochem. 79 (2000) 31;
(b) T.D.P. Stack, V. Mahadevan, M.J. Henson, J.L. Du Bois, B. Hedman, K.O. Hodgson, E.I. Solomon, J. Inorg. Biochem. 86 (2001) 442;
(c) Y.F. Song, C. Massera, P. Gamez, A.M.M. Lanfredi, J. Reedijk, Eur. J. Inorg. Chem. (2004) 3025.
[9] (a) S.M. Morehouse, A. Polychronopoulou, G.J.B. Williams, Inorg Chem. 19 (12) (1980) 3558–3561;
(b) G. Fransson, B.K.S. Lundberg, Acta Chem. Scand. A 28 (5) (1974) 578–588;
(c) D.L. McFadden, A.T. McPhail, C.D. Garner, F.E. Mabbs, J. Chem. Soc., Dalton Trans. (1976) 47–52.
[10] H. Beinert, Coord. Chem. Rev. 33 (1980) 55.
[11] J.R.J. Sorrenson, Prog. Med. Chem. 26 (1989) 437 (and references therein).
[12] A.L. Abuhijleh, C. Woods, Inorg. Chim. Acta 209 (1993) 187.
[13] H. Tamura, H. Imai, J. Kuwahara, Y. Sugiura, J. Am. Chem. Soc 109 (1987) 6870.
[14] C.P. Raptopoulu, S. Paschalidou, A.A. Pantazaki, A. Terzis, S.P. Perlepes, T. Lialiaris, E.G. Bakalbassis, J. Mrozinski, D.A. Kyriakidis, J. Inorg. Biochem. 71 (1998) 15.
[15] (a) J. Server-Carrió, E. Eseriva, J.-V. Folgado, Trans. Met. Chem. 21 (1996) 541–545;
(b) E. Suresh, J. Chem. Cryst. 39 (2009) 104;
(c) A.S. Antsyshkina, G.G. Sadikov, A.L. Poznyak, V.S. Sergienko, Russ. J. Inorg. Chem. 51 (2006) 283;
(d) X. You, L. Zhu, J. Sun, Chin. J. Chem. 28 (2010) 2174;
(e) C.K. Prout, G.B. Allison, F.J.C. Rossotti, J. Chem. Soc. A (1971) 3331–3335;
(f) R. Koner, I. Goldberg, Acta Cryst. C65 (2009) m37;
(g) J.K. Nath, A.M. Kirillov, J.B. Baruah, RSC Adv. 4 (2014) 47876;
(h) L.-Q. Xiao, J.-Z. Qiao, T.-P. Hu, Chin. J. Inorg. Chem. 30 (2014) 2127;
(i) A.L. Abuhijleh, C. Woods, Inorg. Chim. Acta 194 (1992) 9;
(j) D.-D. Lin, D.-J. Xu, J. Coord. Chem. 58 (2005) 605.
[16] (a) S. Wang, M.-L. Hu, J.-X. Yuan, Y.-Q. Cheng, J.-J. Lin, Z.-Y. Huang, Chin. J. Chem. 18 (2000) 546;
(b) A. Benkanoun, F. Balegroune, A. Guehria-Laidoudi, S. Dahaoui, C. Lecomte, Acta Cryst. E68 (2012) m480;
(c) Y. Wu, L. Yu, M. Cheng, W. Han, L. Wang, X. Guo, Q. Liu, Chin. J. Chem. 1045 (2012) 30;
(d) E. Suresh, M.M. Bhadbhade, K. Venkatasubramanian, Polyhedron 18 (1999) 657;
(e) Z.M. Jin, L. He, L. Shen, M.C. Li, M.L. Hu, Acta Cryst. E59 (2003) m1053;
(f) K.-L. Zhang, H.-W. Kuai, W.-L. Liu, G.-W. Diao, J. Mol. Struct. 831 (2007) 114.
[17] (a) D.-D. Lin, D.-J. Xu, Acta Cryst E61 (2005) m1215;
(b) Y.-Q. Cheng, W.-J. Lin, M.-L. Hu, J.-X. Yuan, S. Wang, J.-G. Wang, Chin. J. Chem 19 (2001) 321;
(c) I.G. Filippova, O.A. Gerco, Y.A. Simonov, A.A. Deseatnic-Ciloci, S.F. Clapco, J. P. Tiurin, S.G. Baca, Polyhedron 29 (2010) 1102;
(d) F. Guo, X. Zhang, B. Zhu, J. Qiu, J. Inorg. Organomet. Polym. Mater 20 (2010) 38;
(e) D. Cheng, M.A. Khan, R.P. Houser, Inorg. Chim. Acta 351 (2003) 242;
(f) P. Naumov, M. Ristova, M.G.B. Drew, S.W. Ng, Acta Cryst C56 (2000) e372;
(g) Q. Zhang, C. Lu, J. Chem. Cryst 35 (2005) 965;
(h) K.-L. Zhang, G.-W. Diao, S.W. Ng, Acta Cryst. (2010) E66. m1430;

(i) Y.-J. Wang, Y.-Y. Wang, J. Feng, Q.-Y. Lin, Z. Kristallogr 224 (2009) 549;
(j) L.-P. Sun, S.-Y. Niu, J. Jin, G.-D. Yang, L. Ye, Inorg. Chem. Commun 9 (2006) 679.
[18] (a) N. Zhao, Z. Lian, T. Lou, J. Zhang, X. Li, P. Liu, Z. Kristallogr. 224 (2009) 463;
(b) M. Hu, D. Cheng, J. Liu, D. Xu, J. Coord. Chem. 53 (2001) 7;
(c) Y.-D. Wang, X.-H. Wu, Q.-X. Zeng, Y.-W. Yao, Chin. J. Struct. Chem. 24 (2005) 641;
(d) J.-R. Su, K.-L. Yin, D.-J. Xu, Chin. J. Struct. Chem. 23 (2004) 399;
(e) H.-J. Chen, Y.-G. Li, J. Coord. Chem. 61 (2008) 2150.
[19] (a) L. Yue, Q.-X. Zhou, Y.-J. Wang, X.-Q. Zhao, Chin. J. Struct. Chem 24 (2005) 287;
(b) C. An, X. Feng, N. Zhao, P. Liu, T. Wang, Z. Lian, J. Cluster Sci. 26 (2015) 889;
(c) S. Gao, J.-W. Liu, L.-H. Huo, H. Zhao, J.-G. Zhao, Acta Cryst. E60 (2004) m1308;
(d) G. Gunay, O.Z. Yesilel, C. Darcan, S. Keskin, O. Buyukgungor, Inorg. Chim. Acta 399 (2013) 19.
[20] C. Sudha, S.K. Mandal, A.R. Chakravarty, Inorg. Chem. 37 (1998) 270.
[21] Y.-F. Deng, Z.-H. Zhou, Z.-X. Cao, K.-R. Tsai, J. Inorg. Biochem. 98 (2004) 1110.
[22] G.A. Bain, J.F. Berry, J. Chem. Educ. 85 (2008) 532–536.
[23] APEX2, SADABS and SAINT. Bruker AXS Inc., Madison, Wisconsin, USA. 2008.
[24] L.J. Farrugia, J. Appl. Cryst. 45 (2012) 849–854.
[25] M.C. Burla, R. Caliandro, B. Carrozzini, G.L. Cascarano, C. Cuocci, C. Giacovazzo, M. Mallamo, A. Mazzone, G. Polidori, J. Appl. Cryst. 48 (2015) 306–309.
[26] G.M. Sheldrick, Acta Cryst. C71 (2015) 3–8.
[27] C.F. Macrae, I.J. Bruno, J.A. Chisholm, P.R. Edgington, P. McCabe, E. Pidcock, L. Rodriguez-Monge, R. Taylor, J. van de Streek, P.A. Wood, J. Appl. Cryst. 41 (2008) 466–470.
[28] S.P. Westrip, J. Appl. Cryst. 43 (2010) 920–925.
[29] R. Dennington, T. Keith, J. Millam, GaussView, Version 5, Semichem Inc., Shawnee Mission, KS, 2009.
[30] M. J. Frisch, G. W. Trucks, H. B. Schlegel, G. E. Scuseria, M. A. Robb, J. R. Cheeseman, G. Scalmani, V. Barone, B. Mennucci, G. A. Petersson, H. Nakatsuji, M. Caricato, X. Li, H. P. Hratchian, A. F. Izmaylov, J. Bloino, G. Zheng, J. L. Sonnenberg, M. Hada, M. Ehara, K. Toyota, R. Fukuda, J. Hasegawa, M. Ishida, T. Nakajima, Y. Honda, O. Kitao, H. Nakai, T. Vreven, J. A. Montgomery, Jr., J. E. Peralta, F. Ogliaro, M. Bearpark, J. J. Heyd, E. Brothers, K. N. Kudin, V. N. Staroverov, R. Kobayashi, J. Normand, K. Raghavachari, A. Rendell, J. C. Burant, S. S. Iyengar, J. Tomasi, M. Cossi, N. Rega, J. M. Millam, M. Klene, J. E. Knox, J. B. Cross, V. Bakken, C. Adamo, J. Jaramillo, R. Gomperts, R. E. Stratmann, O. Yazyev, A. J. Austin, R. Cammi, C. Pomelli, J. W. Ochterski, R. L. Martin, K. Morokuma, V. G. Zakrzewski, G. A. Voth, P. Salvador, J. J. Dannenberg, S. Dapprich, A. D. Daniels, Ö. Farkas, J. B. Foresman, J. V. Ortiz, J. Cioslowski & D. J. Fox, Gaussian 09, Revision A.02, Gaussian, Inc., Wallingford CT, 2009.
[31] A.W. Addison, T.N. Rao, J. Reedijk, J. van Rijn, G.C. Verschoor, J. Chem. Soc., Dalton Trans. (1984) 1349.
[32] J. Sanchiz, Y. Rodríguez-Martín, C. Ruiz-Pérez, A. Mederos, F. Lloret, M. Julve, New J. Chem. 26 (2002) 1624–1628.
[33] R. Carballo, A. Castiñeiras, B. Covelo, E. García-Martínez, J. Niclós, E.M. Vázquez-López, Polyhedron 23 (2004) 1505–1518.
[34] A.T. Çolak, F. Çolak, D. Akduman, O.Z. Yeşilel, O. Büyükgüngör, Solid State Sci. 11 (2009) 1908–1918.
[35] (a) A.L. Abuhijleh, C. Woods, Inorg. Chem. Commun. 4 (2001) 119–123;
(b) A. Vlad, M.-F. Zaltariov, S. Shova, G. Novitchi, C.-D. Varganici, C. Train, M. Cazacu, CrystEngComm 1 (5) (2013) 5368–5375;
(c) W. Wolodkiewicz, J. Coord. Chem. 55 (2002) 727.
[36] G. Zhang, G. Yang, J.S. Ma, Cryst. Growth Des. 6 (2006) 375.
[37] R. Moreno-Fuquen, J. Ellena, J.E. Theodoro, Acta Cryst. E65 (2009) o2717.
[38] V.H. Rodrigues, M.M.R.R. Costa, E. de Matos Gomes, M.S. Belsley, Acta Cryst. (2007) E63. o4031.
[39] D.-J. Yang, Acta Cryst. E63 (2007) o4038.
[40] D.-D. Lin, J.-G. Liu, D.-J. Xu, Acta Cryst. E62 (2006) o451–o452.
[41] Z.-X. Liu, Acta Cryst. E65 (2009) o499.
[42] R.C. Bott, D.S. Sagatys, D.E. Lynch, G. Smith, C.H.L. Kennard, T.C.W. Mak, Aust. J. Chem. 44 (1991) 1495–1498.
[43] M.T.M. Al-Dajani, H.H. Abdallah, N. Mohamed, C.S. Yeap, H.-K. Fun, Acta Cryst. E65 (2009) m1540–m1541.
[44] J. Bernstein, R.E. Davis, L. Shimoni, N.-L. Chang, Angew. Chem. Int. Ed. Engl. 34 (1995) 1555–1573.
[45] M.A. Spackman, D. Jayatilaka, CrystEngComm 11 (2009) 19–32.
[46] M. Spackman, J.J. McKinnon, Cryst Eng Comm. 4 (2002) 378.
[47] S.K. Wolff, D.J. Grimwood, J.J. McKinnon, M.J. Turner, D. Jayatilaka, M.A. Spackman, Crystal Explorer, University of Western Australia, Perth, 2012.
[48] B. Guillot, E. Enrique, L. Huder, C. Jelsch, Acta Cryst. A70 (2014) C279.
[49] C. Jelsch, K. Ejsmont, L. Huder, IUCrJ 1 (2014) 119.
[50] (a) W.E. Klee, Cryst. Res. Technol. 39 (2004) 959–968;
(b) J.-G. Eon, Acta Cryst. A61 (2005) 501–511;
(c) O. Delgado-Friedrichs, M. O'Keeffe, J. Solid State Chem. 178 (2005) 2480–2485.
[51] (a) A. F. Wells, Three-Dimensional Nets and Polyhedra, 1977, New York: Interscience. (b) L. Öhrström & K. Larsson, Molecule-Based Materials: The Structural Network Approach, 2005, Amsterdam: Elsevier. (c) L. Carlucci, G. Ciani & D. M. Proserpio, Making Crystals by Design. Methods, Techniques and Applications, 2007, Edited by D. Braga & F. Grepioni, Wiley : Darmstadt.
[52] V.A. Blatov, A.P. Shevchenko, D.M. Proserpio, Cryst. Growth Des. 14 (2014) 3576–3586.
[53] P. Che, D. Fang, D. Zhang, J. Feng, J. Wang, N. Hu, J. Meng, J. Coord. Chem. 58 (17) (2005) 1581–1588.
[54] Y.-F. Deng, Z.-H. Zhou, J. Coord. Chem. 62 (5) (2009) 778–788.
[55] (a) L. Bellamy, The Infrared Spectra of Complex Molecules, Wiley, New York, 1958;
(b) L.C. Bichara, H.E. Lanús, E.G. Ferrer, M.B. Gramajo, S.A. Brandán, Advan. Phys. Chem. 347072 (2011) 1–10;
(c) R.-H. Zhang, X.-W. Zhou, Y.-C. Guo, M.-L. Chen, Z.-X. Cao, Y.L. Chow, Z.-H. Zhou, Inorg. Chim. Acta 406 (2013) 27–36.
[56] A. Selvam, S. Pandi, S. Selvakumar, S. Srinivasan, Arch. Appl. Sci. Res. 4 (6) (2012) 2474–2478.
[57] H.-J. Chen, J. Zhang, W.-L. Feng, M. Fu, Inorg. Chem. Commun. 9 (2006) 300–303.
[58] R. Ramasamy, Armenian J. Phys. 8 (1) (2015) 51–55.
[59] B. Morzyk-Ociepa, E. Rózycka-Sokołowska, D. Michalska, J. Mol. Struct. 1028 (2012) 49–56.
[60] V. Krishnakumar, R. Ramasamy, Indian J. Pure Appl. Phys 40 (2002) 252.
[61] A.S. Mahdi, A.A. Awad, M.M. Hasson, Acta Chim. Pharm. Indica 7 (1) (2017) 1–7.
[62] Y. Anjaneyulu, R.P. Rao, Synth. React. Inorg. Met. Org. Chem. 16 (1986) 257.
[63] M. Montazerozohori, S. Zahedi, M.N. Esfahani, A. Naghiha, J. Ind. Eng. Chem. 20 (2014) 2463.
[64] S.A. Sadeek, W.H. El-Shwiniy, M.S. El-Attar, Spectrochim. Acta, Part A 84 (2011) 99.
[65] R. Moutafchieva, D. Yarkov, J. Sci. 4 (3) (2006) 28.
[66] A.A. Soayed, H.M. Refaat, D.A. Noor El-Din, Inorg. Chim. Acta 406 (2013) 230–240.
[67] A.A. Soayed, H.M. Refaat, D.A. Noor El-Din, Inorg. Chim. Acta 421 (2014) 59–66.
[68] H. Erer, O.Z. Yeşilel, C. Darcan, O. Büyükgüngör, Polyhedron 28 (2009) 3087–3093.

sev and pcu Topological Nets in One-Pot Newly Synthesized Mixed-ligand Imidazole-containing Cu(II) Coordination Frameworks: Crystal Structure, Intermolecular Interactions, Theoretical Calculations, Magnetic Behavior and Biological Activity

Amani Direm[a*], Mohammed S. M. Abdelbaky[b], Koray Sayın[c], Andrea Cornia[d], Olufunso Abosede[e] & Santiago García-Granda[b].

[a] Laboratoire des Structures, Propriétés et Interactions Interatomiques LASPI^{2}A, Département des Sciences de la Matière, Faculté des Sciences et de la Technologie, Université ‘’Abbes Laghrour’’, Khenchela 40.000, Algeria.

[b] Departamentos de Química Física y Analítica, Universidad de Oviedo – CINN, 33006 Oviedo, Spain.

[c] Department of Chemistry, Faculty of Science, Cumhuriyet University 58140 Sivas, Turkey.

[d] Dipartimento di Scienze Chimiche e Geologiche, Università di Modena e Reggio Emilia & INSTM, via G. Campi 103, 41125 Modena, Italy.

[e] Department of Chemistry, Federal University Otuoke, P.M.B 126, Yenagoa, Bayelsa State, Nigeria.

* Corresponding Author : Amani Direm

E-mail : amani_direm@yahoo.fr

Tel. : +213.772.33.02.87

Experimental :

Magnetic measurements

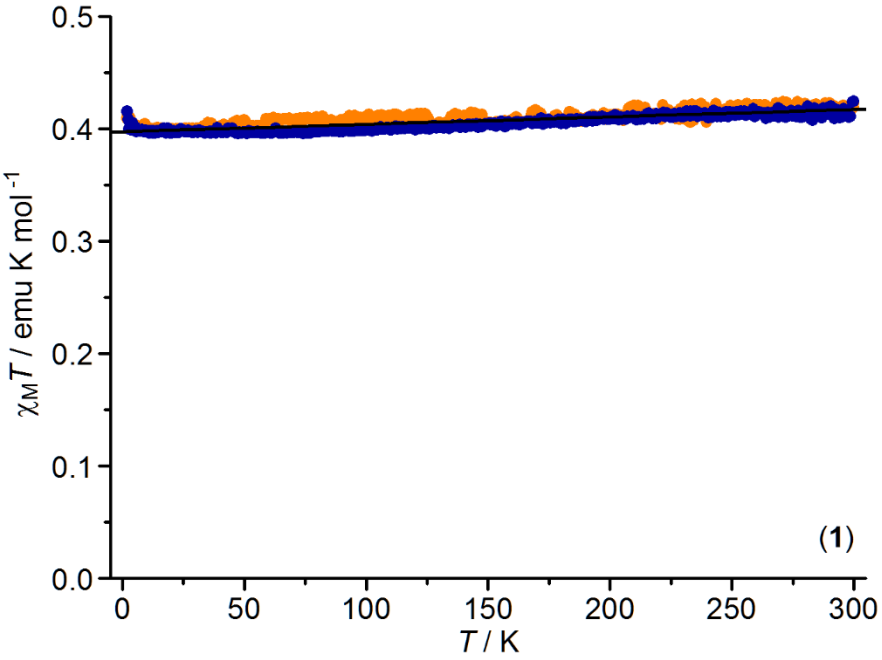

Figure S1. $\chi_M T$ *versus* T data for compound (**1**), measured in an applied field of 1 kOe with increasing (orange) or decreasing temperature (blue). A linear fit to the data (black line) provides a Curie constant (intercept) of 0.3973(2) emu K mol^{-1} and a temperature independent contribution to susceptibility (slope) of $6.63(14)\cdot10^{-5}$ emu mol^{-1}.

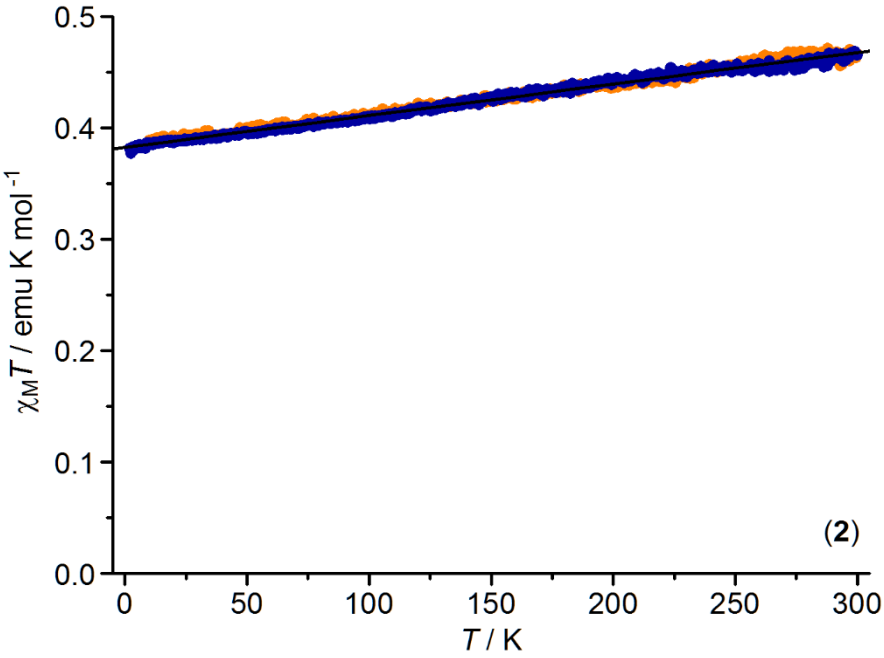

Figure S2. $\chi_M T$ *versus* T data for compound (**2**), measured in an applied field of 1 kOe with increasing (orange) or decreasing temperature (blue). A linear fit to the data (black line) provides a Curie constant (intercept) of 0.38250(15) emu K mol^{-1} and a temperature independent contribution to susceptibility (slope) of $2.836(8)\cdot10^{-4}$ emu mol^{-1}.

X-ray single-crystal structure analysis

Table S1.

Crystal data and structure refinement parameters for complexes (**1**) and (**2**).

Crystal Data	Complex (**1**)	Complex (**2**)
Chemical formula	$C_{15}H_{18}N_6O_7Cu$	$C_{15}H_{18}N_6O_7Cu$
Formula weight ($g \cdot mol^{-1}$)	457.89	457.89
Crystal system	Monoclinic	Triclinic
Space group	$P2_1/n$	P-1
Temperature (K)	298	298
Unit cell dimensions (Å,°) a b c α β γ	 9.0360(2), 23.6063(5), 9.0842(2), - 110.257(1) -	 9.2169 (4), 9.3738 (4), 11.8153 (5), 87.704 (1), 83.425 (1), 64.936 (1)
Volume ($Å^3$)	1817.87(7)	918.56 (7)
Z	4	2
Radiation type	Mo $K\alpha$	Mo $K\alpha$
Calculated density ($g \cdot cm^{-3}$)	1.673	1.656
Absorption coefficient (mm^{-1})	1.26	1.24
Crystal size (mm^3)	0.14 × 0.19 × 0.42	0.16 × 0.23 × 0.63
Color	Light blue-green	Blue
Shape	Prism	Prism
Data collection		
Diffractometer	Bruker–Nonius X8APEX	Bruker–Nonius X8APEX
θ_{max}-θ_{min} (°)	32.0–1.7	32.0–1.7
Measured reflections	29009	11437
Independent reflections	6331	6357
Reflections with $I > 2\sigma(I)$	5272	5369
R_{int}	0.029	0.018
h k l	–13→12 –35→33 –13→13	–13→10 –13→13 –17→16
Refinement		
$R[F^2 > 2\sigma(F^2)]$	0.030	0.033
$wR(F^2)$	0.124	0.128
Goodness of fit	1.17	1.18

Refinement	Complex (**1**)	Complex (**2**)
No. of reflections	6296	6202
No. of parameters	262	262
H-atom treatment	H-atom parameters constrained	H-atom parameters constrained
$\Delta\rho_{max}$, $\Delta\rho_{min}$ (e Å^{-3})	0.68, –1.11	0.79, –0.82

Results and Discussion

X-ray crystallographic study

Hirshfeld Surface analysis

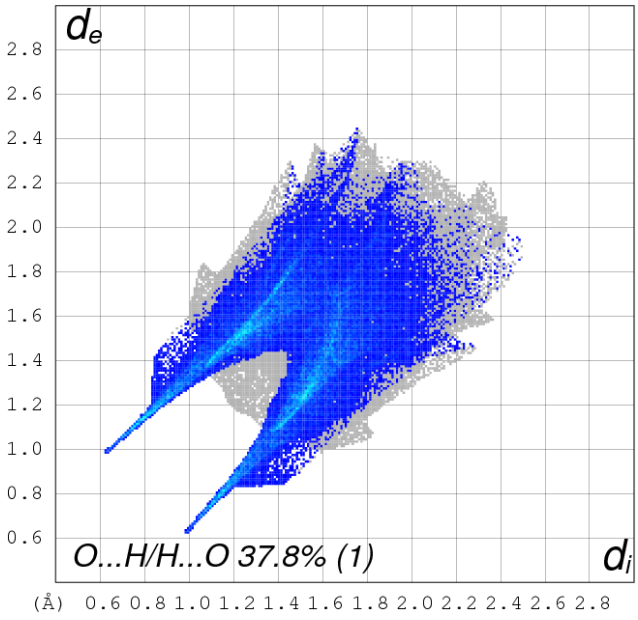

(a)

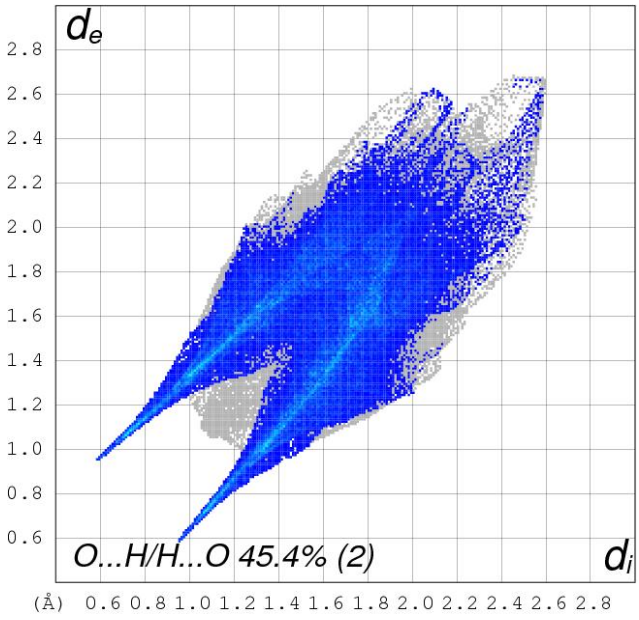

(b)

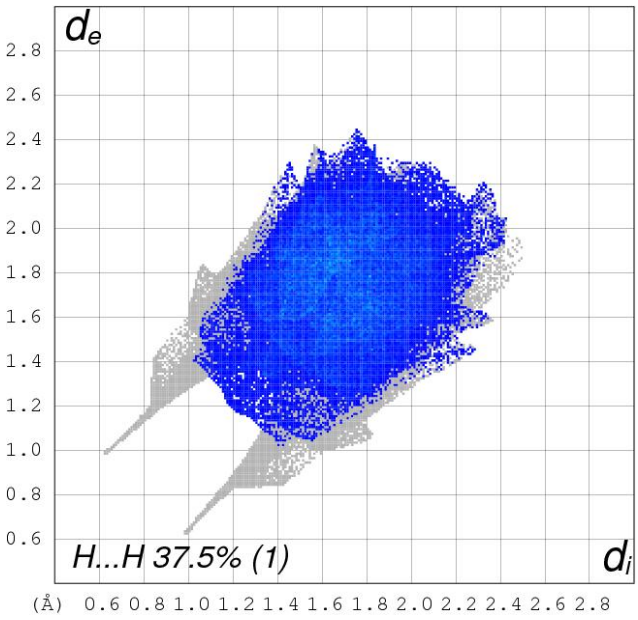

(c)

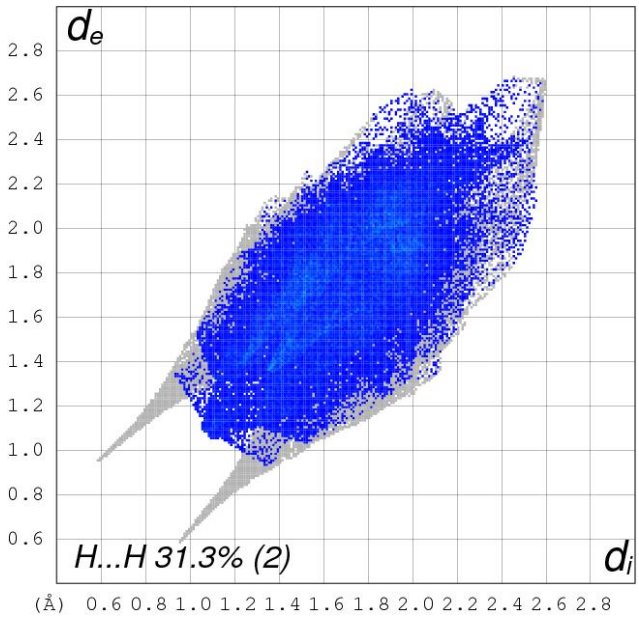

(d)

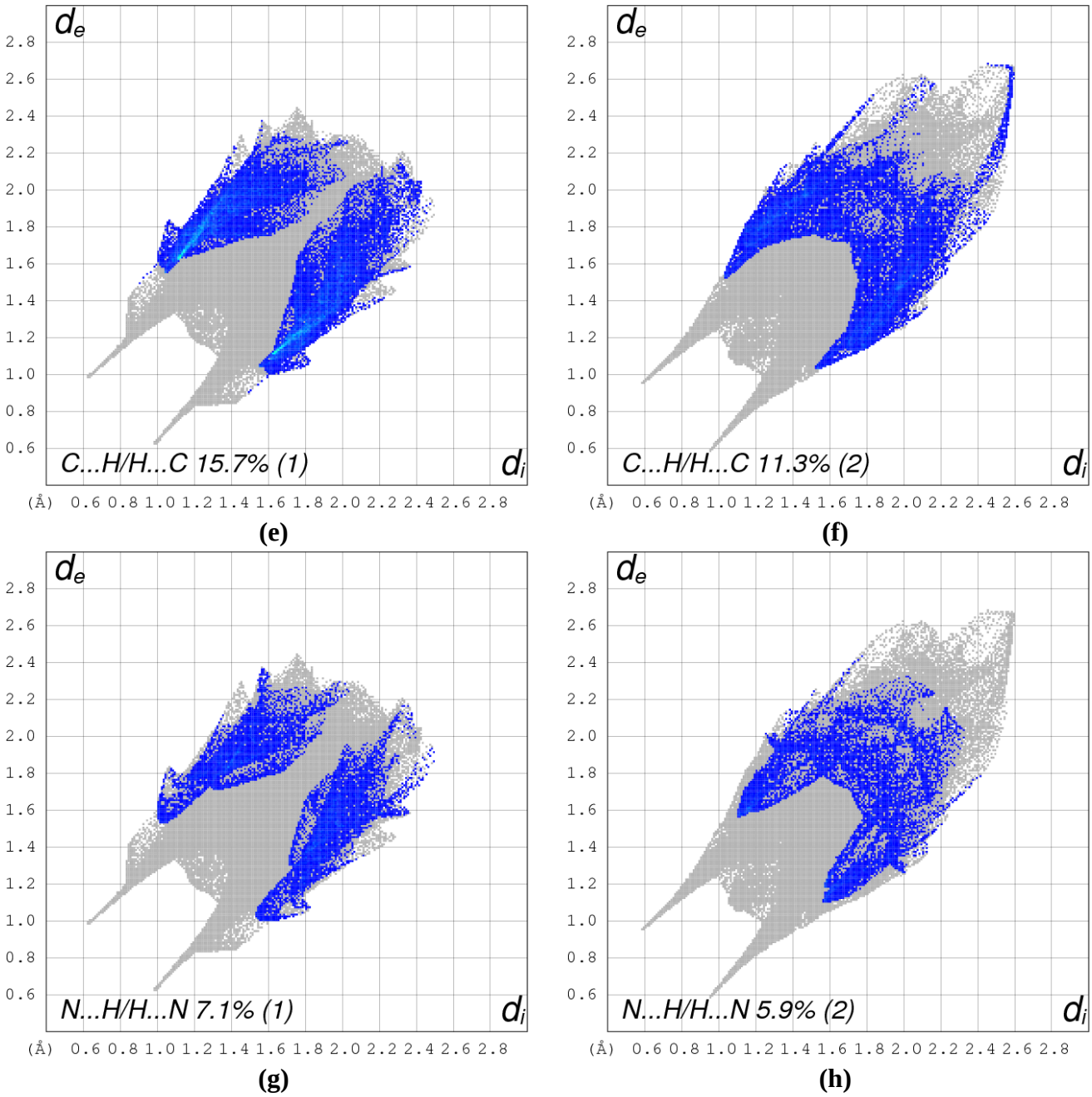

Figure S3. Full 2D-fingerprint plots decomposition into (a), (b) O···H/H···O, (c), (d) H···H, (e), (f) C···H/H···C and (g), (h) N···H/H···N contacts in (**1**) and (**2**).

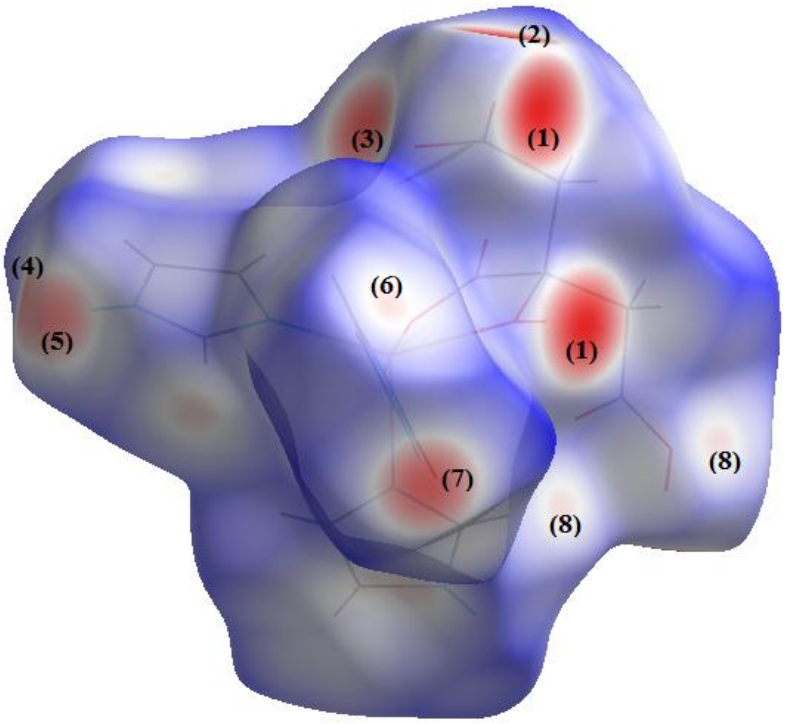

(a)

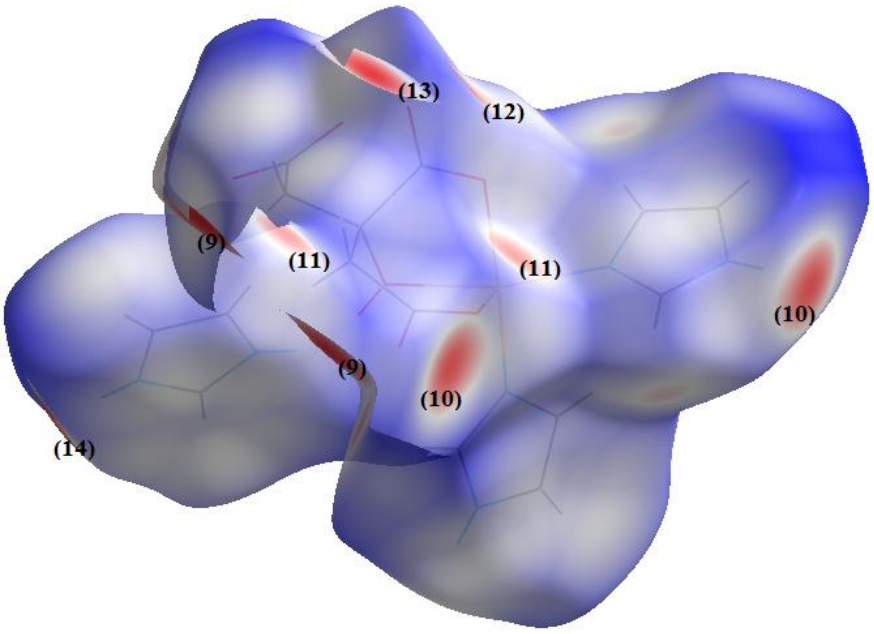

(b)

Figure S4. d_{norm} property mapped on the *Hirshfeld* surfaces of compounds (**1**) and (**2**). (a) The features (1), (2), (3), (4), (5), (6), (7) and (8) describe the interactions O7–H7···O3/O3···H7–O7, O3···H2–O2, O4···H2NA–N2A, N2B–H2NB···O5, N2B–H2NB···O6, C1A–H1A···O1, N2C–H2NC···O4 and C1A–H1A···O2/O2···H1A–C1A. (b) The following features (9), (10), (11), (12), (13) and (14) define the interactions O7–H7···O3/O3···H7–O7, N2A–H2NA···O2/O2···H2NA–N2A, C3C–H3C···O1/O1···H3C–C3C, O5···H2B–C2B, O4···H2NB–N2B and O5···H2NC–N2C, respectively.

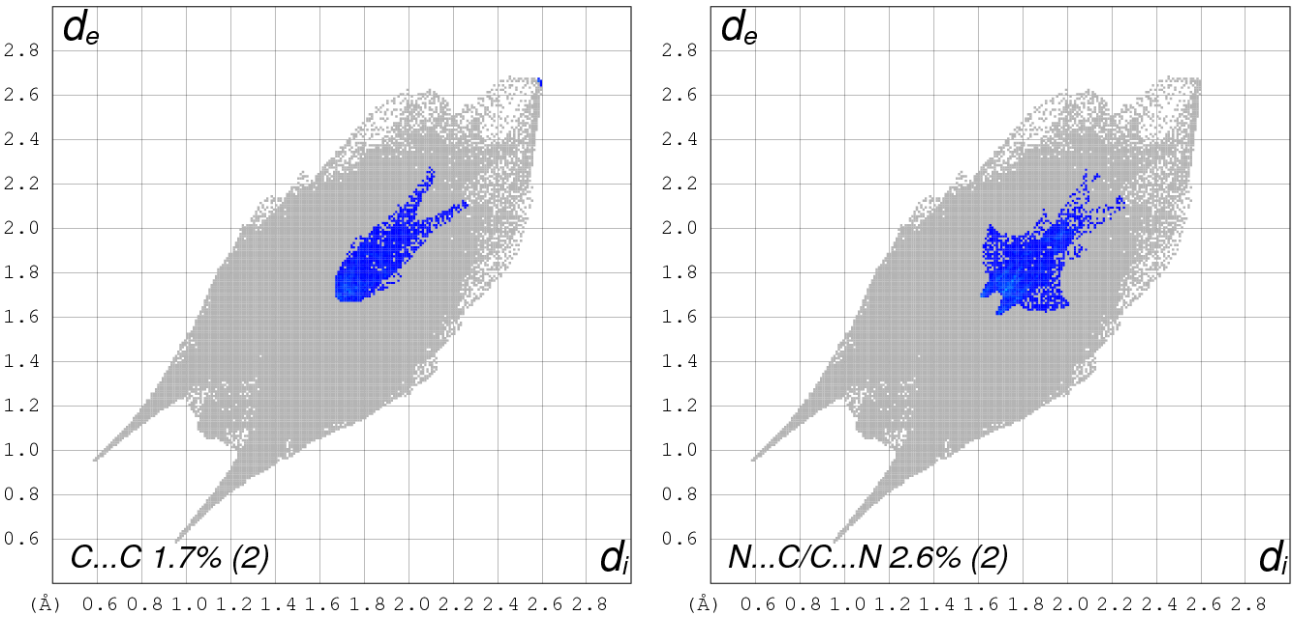

(a) **(b)**

Figure S5. Fingerprint plots of compound (**2**) resolved into (a) C···C contacts and (b) N···C/C···N contacts.

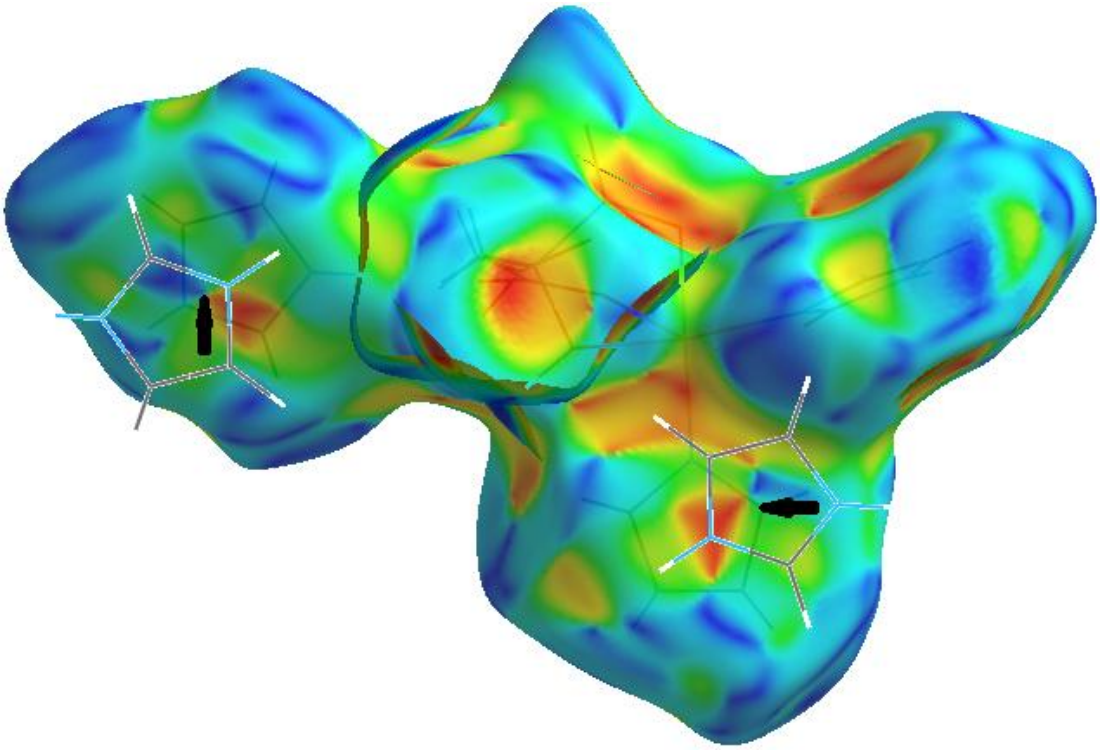

Figure 6S. Shape-index property mapped on the *Hirshfeld* surface around (**2**).

Enrichment ratio

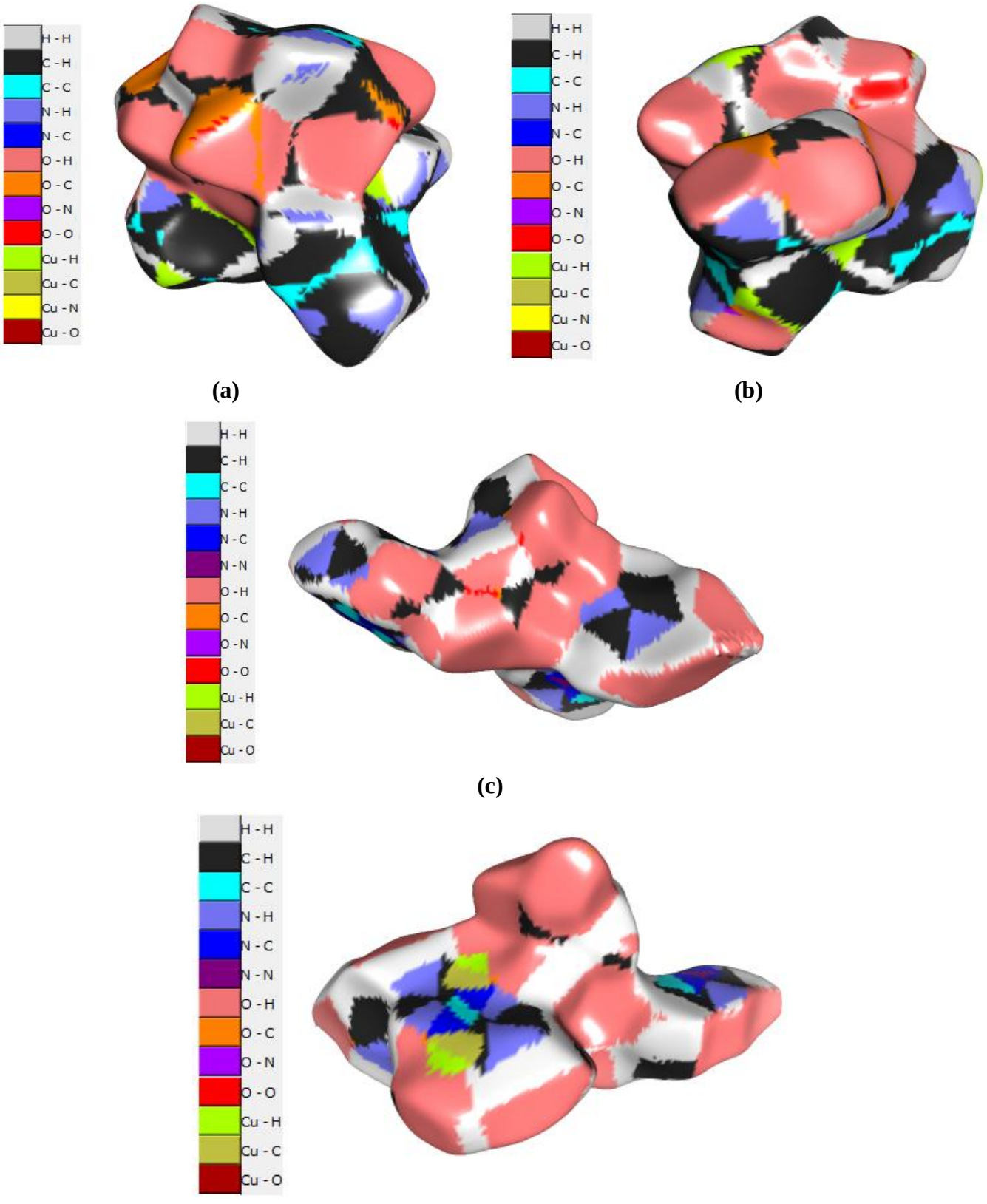

Figure S7. (a), (c) Front and (b), (d) back views of the *Hirshfeld* surfaces colored following the different contacts nature in (**1**) and (**2**).

Topological analysis

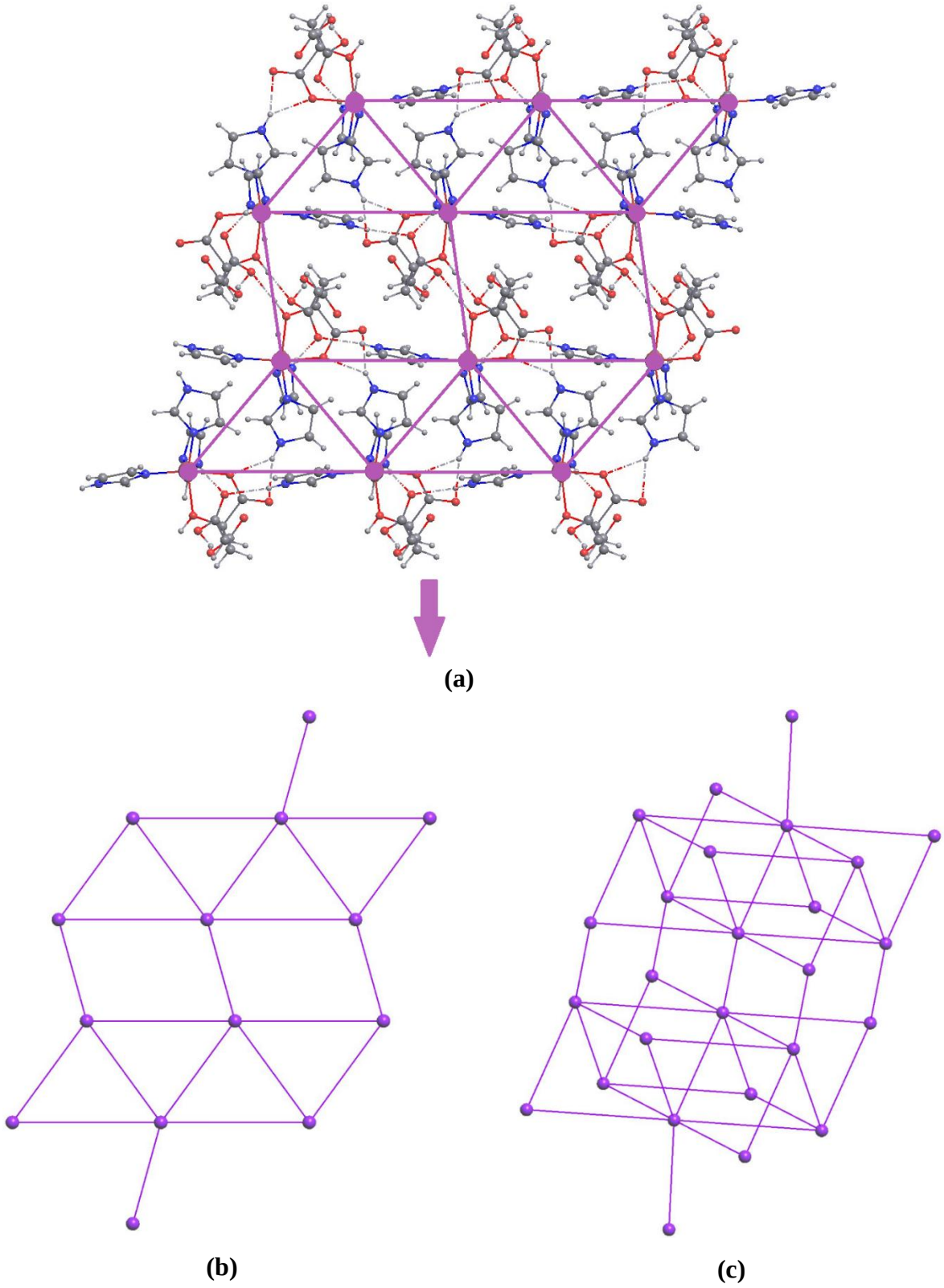

Figure S8. (a) Crystal packing of (**1**) showing the connectivity of each molecule through the hydrogen-bonding frameworks. Standard representation of the crystal structure of (**1**) given (b) along (100) and (c) in a perspective view. The corresponding underlying net is a 7-coordinated **sev.**

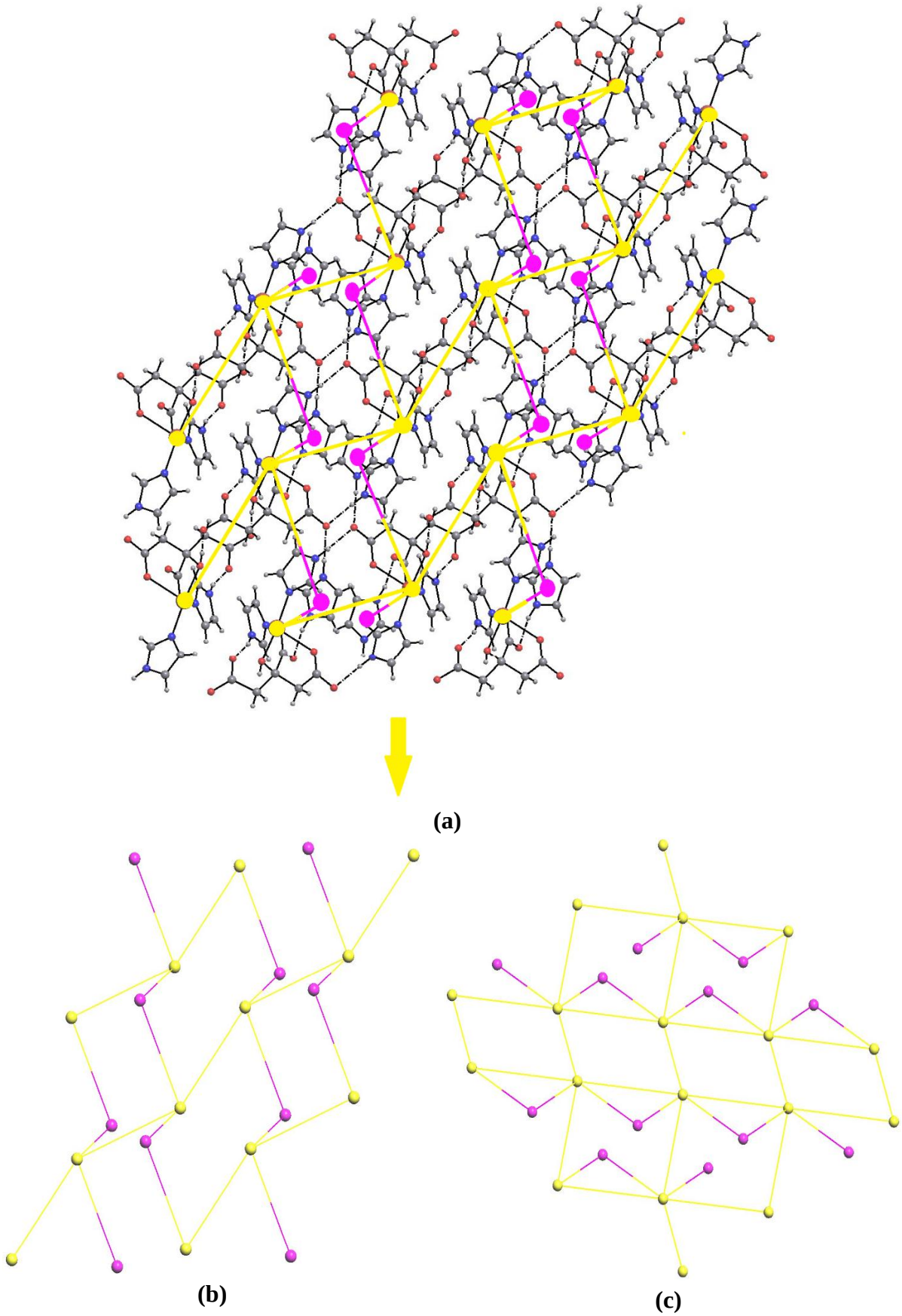

Figure S9. (a) Connectivity of the complex molecules and the imidazolium cations in (**2**). Views of the resulting (2,6)-c binodal 3D-network along the (b) [100] and (c) [010] directions.

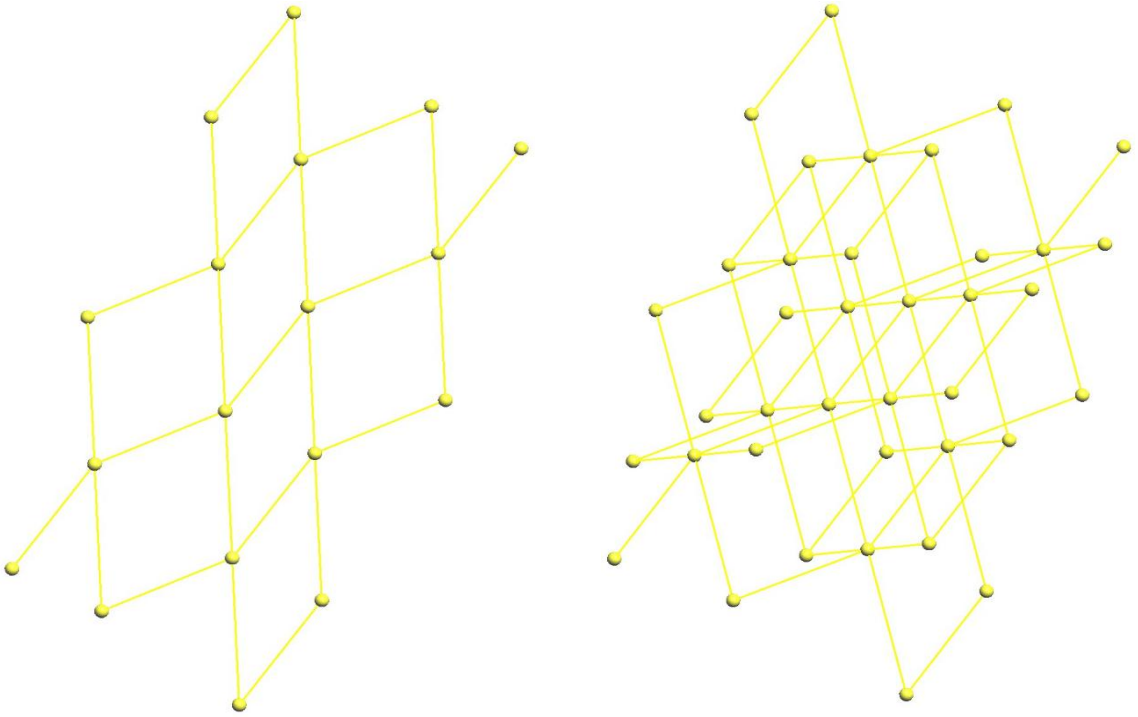

(a) **(b)**

Figure S10. Views (a) along [100] and (b) in perspective of the simplified underlying net for the structure of (**2**), belonging to the **pcu** topology.

Computational Results

Optimized structures

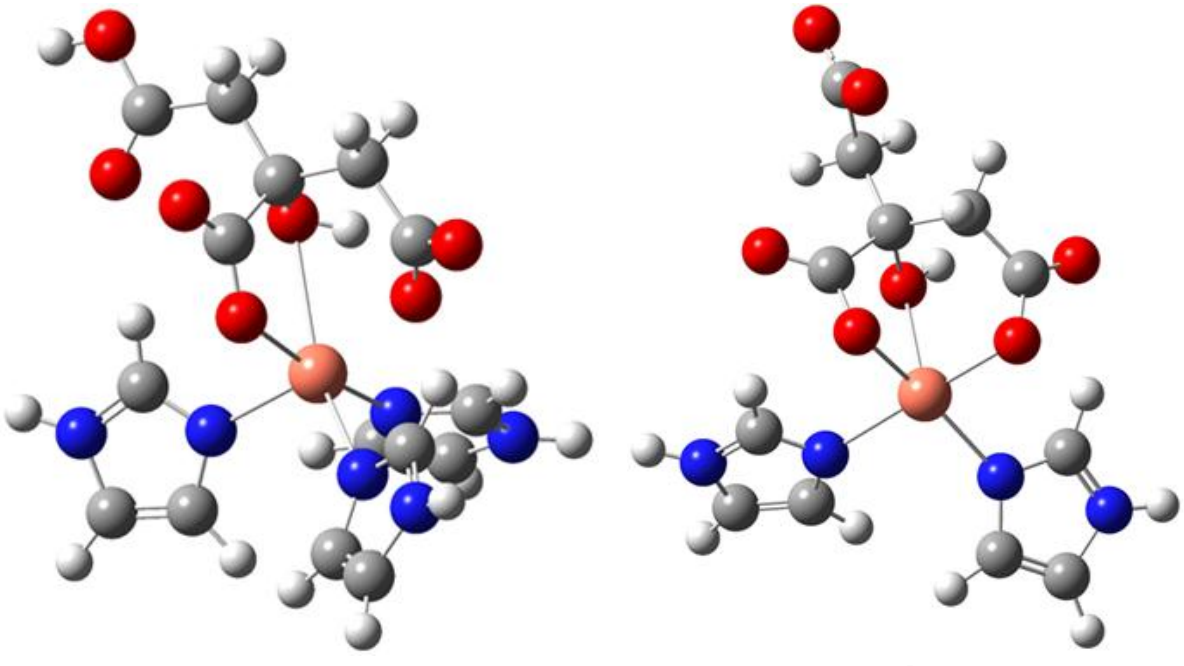

(a) **(b)**

Figure S11. Optimized structures of (a) complex (**1**) and (b) complex (**2**) at HF/6-31G(d)(LANL2DZ) level in the gas phase.

Spectral Analysis

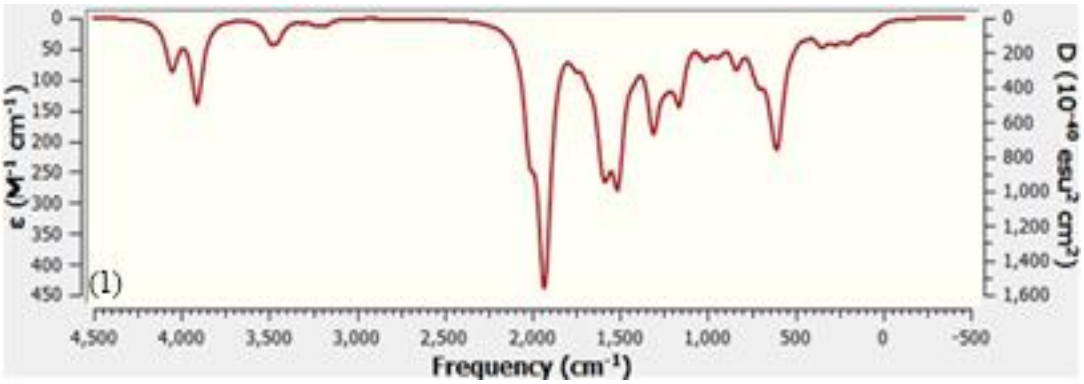

(a)

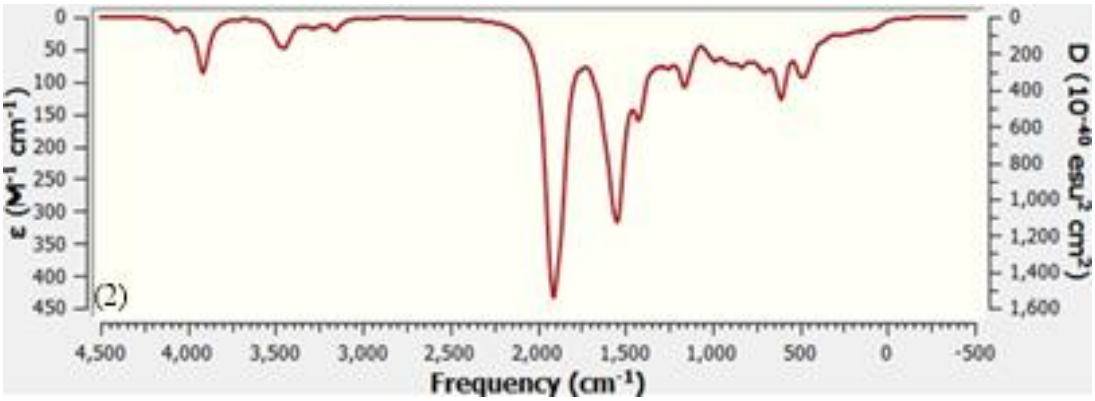

(b)

Figure S12. (a), (b) The calculated infrared spectra of the two complexes.

The NMR spectra of the compounds were calculated with gauge-independent atomic orbital (GIAO) method. In calculation stage of chemical shift values, tetramethylsilane (TMS) was used as a reference substance. Calculated chemical shift values (vs TMS) in the ^{1}H and ^{13}C NMR spectra of the imidazole complexes are gathered in Table S2. Chemical shift values of the aromatic carbon atoms are in the range of 109 – 147 ppm in (**1**) and 109 – 145 ppm in (**2**). Moreover, the citrate carbon signals appear from 41 to 168 ppm and from 45 to 177 ppm in (**1**) and (**2**), respectively. The chemical shift values of the proton signals in the aromatic rings are in the range 5.6 – 11.5 ppm for (**1**) and 5.3 – 8.2 ppm for (**2**). The values 1.2 – 2.8 ppm were obtained for the hydrogen atoms connected to the aliphatic carbons of the two complexes.

Table S2.

^{1}H and ^{13}C NMR chemical shifts (in ppm vs TMS) for (**1**) and (**2**), calculated at the same level of theory.

	^{1}H NMR			^{13}C NMR	
	(**1**)	(**2**)		(**1**)	(**2**)
H2D	2.77	2.09	**C1**	166.95	176.54
H2E	2.49	1.20	**C2**	41.18	44.74
H4A	1.17	2.00	**C3**	66.55	71.25
H4B	1.72	2.81	**C4**	41.44	48.09
H2	5.25	-	**C5**	168.16	159.86
H7	11.18	6.15	**C6**	163.89	166.51
H1A	9.39	7.38	**C1A**	143.86	144.78
H2A	6.51	5.25	**C2A**	110.11	121.19
H3A	6.06	6.15	**C3A**	121.35	108.76
H1B	11.48	8.23	**C1B**	147.03	145.46
H2B	7.93	6.22	**C2B**	112.49	108.45
H3B	10.01	6.25	**C3B**	128.29	122.22
H1C	5.93	-	**C1C**	138.07	-
H2C	6.15	-	**C2C**	109.45	-
H3C	5.55	-	**C3C**	121.71	-
H2NA	7.38	6.85	**-**	-	-
H2NB	8.60	6.83	**-**	-	-
H2NC	6.68	-	**-**	-	-

Spectroscopic IR Study

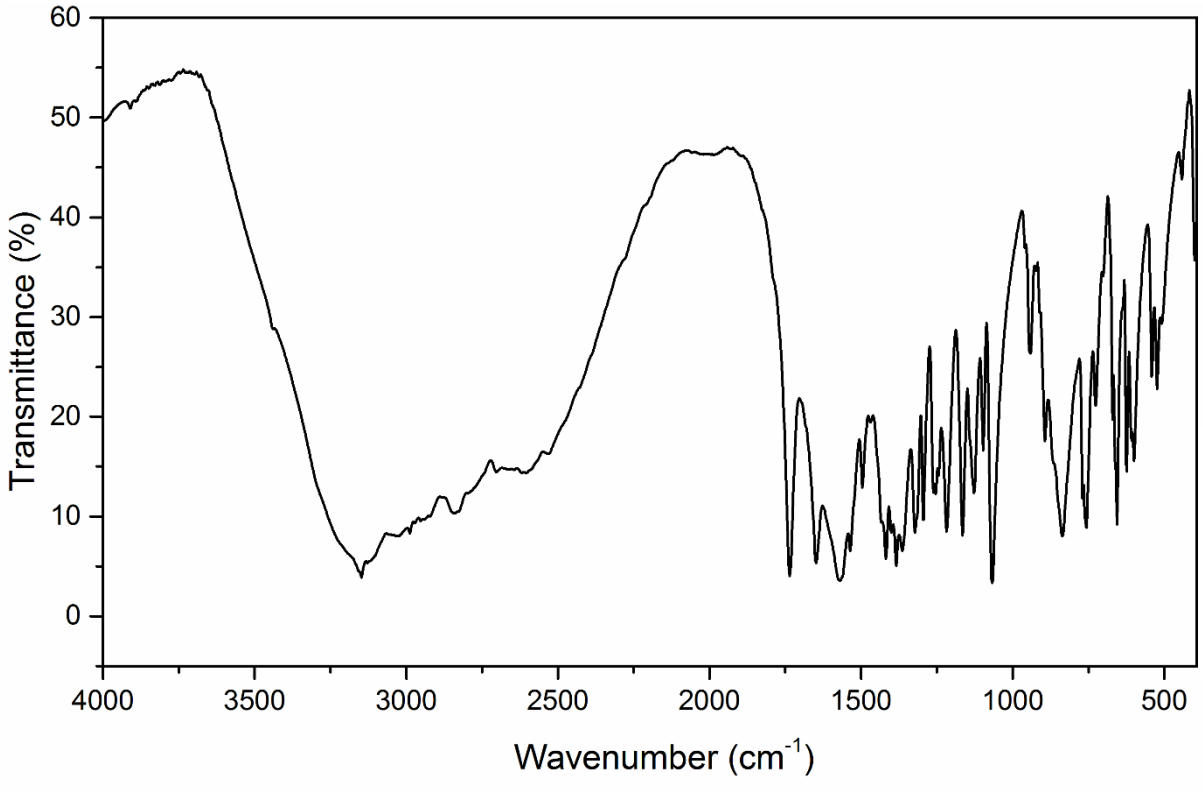

(a)

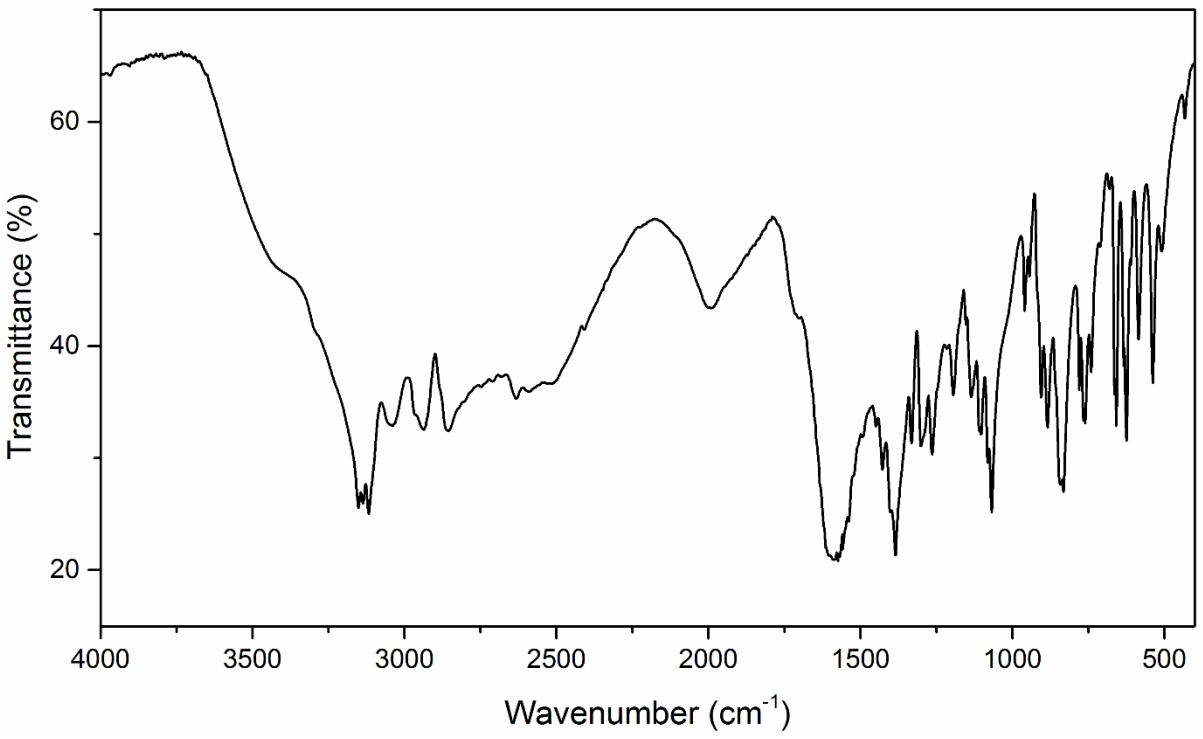

(b)

Figure S13. Infrared spectra of (a) complex (**1**) and (b) complex (**2**).